

SDAC-TR-77-13

12
LEVEL

METHODS OF AUTOMATING ROUTINE ANALYSIS TASKS IN PREPARING A GLOBAL SEISMIC BULLETIN

ADA084190

D.H. von Seggern
Seismic Data Analysis Center
Teledyne Geotech, 314 Montgomery Street, Alexandria Virginia 22314

13 December 1977

APPROVED FOR PUBLIC RELEASE; DISTRIBUTION UNLIMITED.

Sponsored by
The Defense Advanced Research Projects Agency (DARPA)
DARPA Order No. 2151

Monitored By
AFTAC/VSC
312 Montgomery Street, Alexandria, Virginia 22314

DTIC
ELECTE
MAY 7 1980
A

FILE COPY

80 5 5 127

Disclaimer: Neither the Defense Advanced Research Projects Agency nor the Air Force Technical Applications Center will be responsible for information contained herein which has been supplied by other organizations or contractors, and this document is subject to later revision as may be necessary. The views and conclusions presented are those of the authors and should not be interpreted as necessarily representing the official policies, either expressed or implied, of the Defense Advanced Research Projects Agency, the Air Force Technical Applications Center, or the US Government.

Unclassified

SECURITY CLASSIFICATION OF THIS PAGE (When Data Entered)

REPORT DOCUMENTATION PAGE		READ INSTRUCTIONS BEFORE COMPLETING FORM
1. REPORT NUMBER (14) SDAC-TR-77-13	2. GOVT ACCESSION NO. AD-A084290	3. RECIPIENT'S CATALOG NUMBER
4. TITLE (and Subtitle) (6) METHODS OF AUTOMATING ROUTINE ANALYSIS TASKS IN PREPARING A GLOBAL SEISMIC BULLETIN		5. TYPE OF REPORT & PERIOD COVERED (9) Technical Repts
7. AUTHOR(s) (10) D. H. von Seggern		6. PERFORMING ORG. REPORT NUMBER
9. PERFORMING ORGANIZATION NAME AND ADDRESS Teledyne Geotech 314 Montgomery Street Alexandria, Virginia 22314		8. CONTRACT OR GRANT NUMBER(s) (13) F08606-78-C-0007 DARPA Order-2454
11. CONTROLLING OFFICE NAME AND ADDRESS Defense Advanced Research Projects Agency Nuclear Monitoring Research Office 1400 Wilson Blvd. Arlington, Virginia 22209		10. PROGRAM ELEMENT PROJECT TASK AREA & WORK UNIT NUMBER VT/8709 408258
14. MONITORING AGENCY NAME & ADDRESS (if different from Controlling Office) VELA Seismological Center 312 Montgomery Street Alexandria, Virginia 22314 (12) 882		12. REPORT DATE 12/13/77
16. DISTRIBUTION STATEMENT (of this Report) APPROVED FOR PUBLIC RELEASE; DISTRIBUTION UNLIMITED.		13. NUMBER OF PAGES 84
17. DISTRIBUTION STATEMENT (of the abstract entered in Block 20, if different from Report) (11) 13 Dec 77		15. SECURITY CLASS. (of this report) Unclassified
18. SUPPLEMENTARY NOTES		
19. KEY WORDS (Continue on reverse side if necessary and identify by block number) Seismic Analysis Seismic Magnitude Seismic Detection Earthquake Depth Seismic Bulletins		
20. ABSTRACT (Continue on reverse side if necessary and identify by block number) Although it permits more rapid seismic data processing than before being implemented, the Network Event Processing (NEP) system at the Seismic Data Analysis Center could still perform more routine analysis tasks automatically. This report discusses these tasks, including: identification of false alarms in detection lists, timing of P and LR/LQ arrivals, associating seismic arrivals to events, depth-of-focus estimation, and measurement of magnitude. (over)		

DD FORM 1 JAN 73 1473 EDITION OF 1 NOV 65 IS OBSOLETE

Unclassified

SECURITY CLASSIFICATION OF THIS PAGE (When Data Entered)

408258

slb

Unclassified

cont SECURITY CLASSIFICATION OF THIS PAGE(When Data Entered)

Approaches to automating these tasks are presented, tested, and evaluated. Most of the methods are projected to take less time if done automatically than if by human analysts. In particular, the spectral estimation of m_b or M_s is found to be fast and reliable, correlating well with classical analysis estimates. \swarrow

$m \text{ sub } b \text{ or } M \text{ sub } s$

Unclassified

SECURITY CLASSIFICATION OF THIS PAGE(When Data Entered)

Accession For	
NTIS GRA&I	<input checked="checked" type="checkbox"/>
DDC TAB	<input type="checkbox"/>
Unannounced	<input type="checkbox"/>
Justification	
By _____	
Distribution/ _____	
Availability Codes	
Dist <i>A</i>	Avail and/or special

**METHODS OF AUTOMATING ROUTINE ANALYSIS TASKS
IN PREPARING A GLOBAL SEISMIC BULLETIN**

SEISMIC DATA ANALYSIS CENTER REPORT NO.: SDAC-TR-77-13

AFTAC Project Authorization No.:

do not use
VELA T/8709/B/ETR

Project Title:

Seismic Data Analysis Center

ARPA Order No.:

2551

Name of Contractor:

TELEDYNE GEOTECH

Contract No.:

F08606-78-C-0007

Date of Contract:

01 October 1977

Amount of Contract:

\$2,674,245

Contract Expiration Date:

30 September 1978

Project Manager:

Robert R. Blandford
(703) 836-3882

P. O. Box 334, Alexandria, Virginia 22313

APPROVED FOR PUBLIC RELEASE; DISTRIBUTION UNLIMITED.

ABSTRACT

Although it permits more rapid seismic data processing than before being implemented, the Network Event Processing (NEP) system at the Seismic Data Analysis Center, could still perform more routine analysis tasks automatically. This report discusses these tasks, including: identification of false alarms in detection lists, timing of P and LR/LQ arrivals, associating seismic arrivals to events, depth-of-focus estimation, and measurement of magnitude.

Approaches to automating these tasks are presented, tested, and evaluated. Most of the methods are projected to take less time if done automatically than if by human analysts. In particular, the spectral estimation of m_b or M_s is found to be fast and reliable, correlating well with classical analysis estimates.

TABLE OF CONTENTS

	Page
ABSTRACT	2
LIST OF FIGURES	4
LIST OF TABLES	6
INTRODUCTION	7
PREPARATION OF SEISMIC BULLETINS	8
ELIMINATION OF FALSE ALARMS FROM ARRAY DETECTION LOGS	12
Fisher Statistic Verifier	13
Logarithmic Beamforming	17
Spectral Ratio	20
P-WAVE ARRIVAL TIMING	21
LR-WAVE ARRIVAL TIMING	32
AUTOMATIC ASSOCIATION	40
Associating Array Locations	40
NEP Automatic Association	44
DEPTH ESTIMATION	51
Method of Automating pP Depth Determination	52
ESTIMATION OF m_b	60
Justification for a Spectral Estimate	60
Spectral m_b Definition	61
Results for Spectral m_b	63
ESTIMATION OF M_s	71
Definition of a Spectral M_s	71
Results for Spectral M_s	73
CONCLUSION	77
ACKNOWLEDGEMENTS	80
REFERENCES	81

LIST OF FIGURES

Figure No.	Title	Page
1	Schematic of the NEP bulletin operations.	10
2	Example of the processing done to test methods for rejecting false alarms from the LASA detection log.	14
3	Event classification results for the Fisher verifier.	16
4	Event classification results for the logarithmic beaming method.	18
5	Event classification results for the spectral ratio computation.	19
6	P-wave variability as seen at LASA from a small Kamchatka source region (from Blandford and Clark, 1975).	22
7	Signals and noise used in the PE evaluation.	25
8	Flowchart of algorithm to pick exact arrival time and first-motion polarity.	27
9	Example of the start-time determination by STA/LTA and PE algorithms.	30
10	Smart's (1977) processor applied to HGLP and SRO recordings of a Kazakh explosion (04 July 1976).	35
11	Clustering dendrogram for array location estimates of seismic epicenters.	45
12	Basic flowchart of the automatic association program used for preparing the NEP bulletin.	47
13a	NEP bulletin formed by an analyst.	49
13b	NEP bulletin formed by an automatic association program.	50
14	Schematic for the program PPBEAM, an automatic depth determination algorithm.	53
15	Example of the pP incoherent beamforming for depth determination.	55
16	Earthquakes recorded at ANMO and used in determining correlation of spectral-domain and time-domain magnitudes.	64

LIST OF FIGURES (Continued)

Figure No.	Title	Page
17	Correlation of spectral-domain and time-domain body-wave magnitude (m_b) at ANMO for events of Figure 16.	65
18	Body-wave magnitude (m_b) versus the observed period at ANMO for events of Figure 16.	67
19	Correlation of spectral-domain and time-domain surface-wave magnitude (M_s) at ANMO for events of Figure 16.	76

LIST OF TABLES

Table No.	Title	Page
I	Accuracy of P Arrival Time and First-Motion Determination by Automated Means Versus Human Analysts	31
II	Depth Estimation Results from the Automatic pP Beamforming Program PPBEAM	57
III	Automatic Spectral Versus Human Analyst m_b	69
IV	Automatic Spectral Versus Human Analyst M_s	77

INTRODUCTION

Producing a seismic bulletin traditionally requires considerable effort and, in the interest of reliability, the involvement of experienced seismic analysts to obtain the basic data, to check its accuracy and quality, and to associate it with known seismic events. Most of these tasks entail discretionary judgements which have only begun to be, almost reluctantly in some cases, turned over to the appreciably greater speed of computers. This report will identify some of the analyst tasks that may possibly benefit from the application of machine processing in order to reduce the manpower requirements while utilizing objective criteria in performing them. In this report, proposed methods for automating bulletin tasks will be presented and evaluated. While the ideas presented here are not new, taken together they suggest a role for automation that has not been fully used in the preparation of a seismic bulletin. The immediate concern is with its application to the Network Event Processing (NEP) system now operating at the Seismic Data Analysis Center (SDAC), but most of the ideas could be adapted to many systems handling digitized data from seismic networks. The quality and quantity of this data currently reaching the SDAC not only makes these advances possible but in some cases makes their use imperative, especially if near real-time processing is set as a goal.

PREPARATION OF SEISMIC BULLETINS

Traditionally, seismic bulletins were often produced by individuals or small groups whose data came from single stations, and no routine attempts were made to associate the data with seismic events. However, such bulletins were invaluable to more research-oriented seismologists who examined data from worldwide sites and then associated many reported arrivals to a single event. These traditional efforts involved painstaking location computations by hand and culminated in works such as Gutenberg and Richter's (1954) Seismicity of the Earth. This work was, at the time, a monumental achievement, but contemporary seismologists would find much lacking in a bulletin such as Seismicity of the Earth, which had only a m_b threshold of roughly 6.5. Advances in global seismic bulletins came rapidly during the 1960's because of implementing location algorithms on digital computers (Flinn, 1960; Bolt, 1960) and the deployment of the World-Wide Standard Seismograph Network (WWSSN). Personnel at the U.S. Coast and Geodetic Survey in the early 1960's devised procedures to associate data from this new network and to make computer locations of earthquakes worldwide, resulting in a seismic bulletin that approached a 5.0 m_b threshold; the bulletin still appears under the auspices of the U.S. Geological Survey. At the same time, personnel at Teledyne Geotech analyzed and associated data from the Long-Range Seismic Measurements (LRSN) network over North America and produced a bulletin spanning several years of operation. At present, the most extensive data base for worldwide seismic events is found in the International Seismological Summary. All these global bulletins still depend upon human input of seismic phases, their arrival times and amplitudes, as well as considerable human interaction in the definition and location of seismic events. However, more recently, bulletins produced by processing of the data from the Large Aperture Seismic Array (LASA) and the Norwegian Seismic Array (NORSAR) have involved more computer contributions to basic analyst tasks. Detection

Gutenberg, B., and C. F. Richter, 1954. Seismicity of the Earth, 2nd edition: Princeton, Princeton University Press.

Flinn, E. A., 1960. Local earthquake location with an electronic computer, Bull. Seism. Soc. Am., 50, p. 467-470.

Bolt, B. A., 1960. Machine processing of seismic travel-time data, Bull. Seism. Soc. Am., 52, p. 259-263.

of signals, arrival-time determination, amplitude measurement, and depth determination have been done automatically but, except for detections, analysts have routinely overridden these results in preparing the LASA bulletin (Dean et al., 1971), which indicates the inability of automated processes to satisfactorily replace the judgements of human analysts. Elsewhere, an automated system for the Canadian YKA array, described by Weichert and Henger (1976), produces a bulletin that includes estimated locations, arrival times, and amplitudes without analyst interaction. In southern California, a network (Stewart, 1973) produces an automatic seismic bulletin for local events. The proposed operation of a real-time global detection and location based on small arrays is discussed from a data management viewpoint by Shoup and Sax (1975).

The advent of the NEP system has not immediately brought with it many of the latest possibilities for automated processing. The flow of data and the progression of steps in NEP are illustrated in Figure 1. Analysts currently interact with the detections to pick exact arrival times and to measure the amplitudes and periods needed for magnitude computation. They are also required to screen out the numerous false alarms from the array detection logs, as previously done in preparing the LASA bulletin (Chang et al., 1976); and, although certain computer algorithms are available to aid in the task of associating arrivals from different stations to one event and locating that event, the analysts control the actual mechanics of the process. No provisions for automatic handling of long-period data are presently incorporated.

Dean, W. C., and R. O. Ahner, 1971. Evaluation of the SAAC/LASA system. SAAC-1, Teledyne Geotech, Alexandria, Virginia.

Weichert, D. H., and M. Henger, 1976. The Canadian Seismic Array monitor processing system (CANSAM), Bull. Seism. Soc. Am., 66, p. 1381-1404.

Stewart, S. W., 1977. Real-time detection and location of local seismic events in central California, Bull. Seism. Soc. Am., 67, p. 433-452.

Shoup, E. M., and R. L. Sax, 1975. Simulation of a world-wide seismic surveillance network, ALEX(01)-TR-74-13, Texas Instruments, Inc., Dallas, Texas.

Chang, A. C., R. M. Seggelke, and R. R. Baumstark, 1976. Analysis and reduction of false alarms at LASA, SDAC-TR-76-6, Teledyne Geotech, Alexandria, Virginia.

SCHEMATIC OF NETWORK EVENT PROCESSING (NEP)

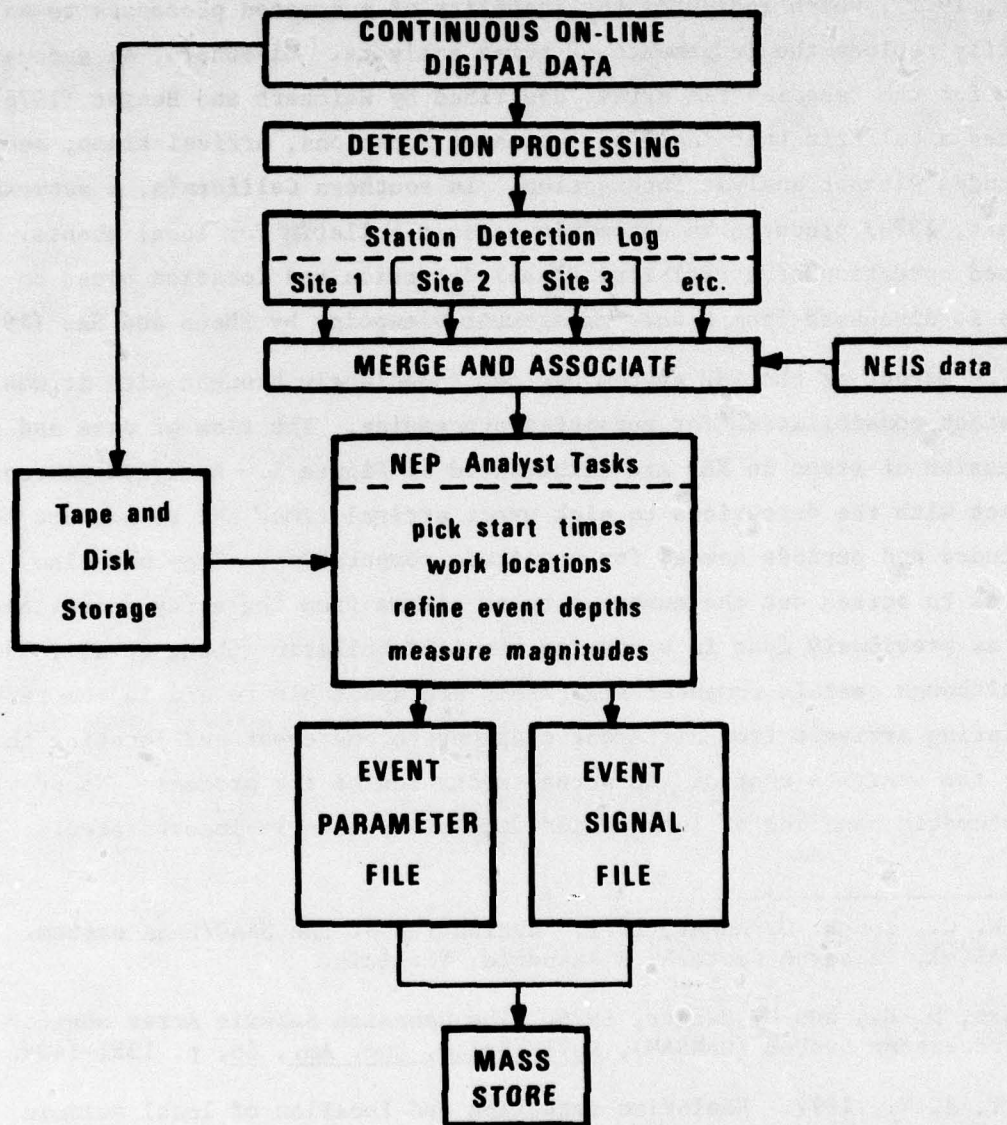


Figure 1. Schematic of the NEP bulletin operations.

As noted before, a future requirement for near real-time processing would necessitate higher reliance on computer-performed processing. Also, the availability and easy access to digital data from stations around the globe can enhance the capability of the analysts to make reliable judgements on the existence of a seismic event and its basic location-magnitude parameters.

This report will discuss some of the possible applications of coded algorithms to the routine analyst tasks and present results which can be used as a basis for judging their worth. The specific topics treated here are: 1) the elimination of false alarms from array detection logs; 2) signal timing (for P and LR waves); 3) automatic association of data; 4) improvement of depth determination by digital waveform processing; and 5) automated measurement of amplitudes to be used in computing the m_b and M_s of an event. No attempt has been made to make an exhaustive investigation of each of these topics. While the methods proposed here are rather simple in concept and practical to implement, the author recognizes that more sophisticated alternatives or modifications will undoubtedly be required as the NFP system evolves.

ELIMINATION OF FALSE ALARMS FROM ARRAY DETECTION LOGS

Chang et al. (1976) studied the nature of the detections output by the LASA event processor and found that roughly one-half can be classified as false alarms. In practice, this figure has been accurate and the seismic analysts have rejected roughly this portion of the EP (event processing) output in producing the LASA Daily Bulletin. Clearly, a reliable screening algorithm would be more efficient, automatically flagging these false alarms before they are presented to the analyst. (Note that such algorithms should not merely counter a poorly designed beam set since a properly designed beam set can prevent only a portion of the false alarms, as shown by Chang et al., 1976.) Also, certain simple algorithms such as "grouping", described in Chang et al., should be operating to eliminate false alarms before the data is subjected to the more time-consuming checks suggested below.

The classification of events by Chang et al. was made according to these seven categories: 1) identified initial phases; 2) identified later phases; 3) duplicate detections (side-lobe or coda detections); 4) regional or local events that are poorly aligned on a regional beam or that are detected on a teleseismic beam; 5) velocity failures ($>$ P-wave velocity); 6) weak signal with poor coherency; 7) detections due to data dropouts, glitches, etc. Out of the seven, categories (1), (2) and (5) can be regarded as valid detections which should be passed to the analyst or perhaps automatic association routines. Category 5 is generally a PKP detection, but it was not used in preparing the LASA bulletin due to the poor epicenter estimate from a high-velocity phase. Of the false alarm categories, duplicate detections (3) were most prevalent; these are typically poorly beamed coda signals, but still have enough power to trip the detection logic. A portion of the LASA event data base was selected out to investigate several possible screening algorithms. This data base comprised 325 events output by EP in the period 08 June to 12 June 1974, a time frame in which Beam Set No. 133 was in operation at the LASA DP (detection processing) level. LASA comprised 13 sub-arrays at this time. Although several algorithms were programmed and used on the data, only three are promising enough to describe here: 1) a Fisher-statistic verifier, 2) logarithmic beaming, and 3) a spectral ratio criterion.

Fisher-Statistic Verifier

The use of the Fisher statistic (F) at TFO as a signal detector (F-detector) has been favorably evaluated by Blandford (1970). Although Blandford (1972) and Blandford and Wirth (1973) provided further theoretical support for this detection logic, the problem with the F-detector is that it requires too much computation time to be practical for any array with a large beam set. However, it would be practical to achieve the benefits of the F-detector without wasting computer power by cascading it onto the normal STA/LTA (short-term average over long-term average) detector for only those time windows with a declared detection. (In view of this proposed application, the procedure is termed a "Fisher verifier" here.) The expression for the F-detector value on an N-channel array is

$$F = \frac{N-1}{N} \frac{\overline{(\sum s_i)^2}}{\sum (s_i - \hat{s})^2}$$

where the s_i 's are the individual, time-delayed channels used in the beam and \hat{s} is the beam estimate itself. The bars indicate averaging over a time window, which was set at 2 sec or twenty sample points, with 50% overlap. The "individual" channels in this case are the 13 subarray beams at LASA.

The processing is exemplified in Figure 2. First the raw data is passed through a 0.9 - 1.4 Hz tight bandpass filter which simulates the actual filtering done in EP processing; traces 1 and 2 show the beams of phased subarrays before and after filtering. Trace 7 is the F-statistic output according to the above relation, using the filtered traces. The arrival of the signal, as declared by the STA/LTA logic, is 30 sec (halfway) into the trace, and the largest F-statistic in the window from 30 to 35 sec into its trace is saved. The DP STA values are displayed in trace 5; these are updated every

Blandford, R. R., 1970. An automatic event detector at TFO, SDL-263, Teledyne Geotech, Alexandria, Virginia.

Blandford, R. R., 1972. Qualitative properties of the F-detector, SDL-291, Teledyne Geotech, Alexandria, Virginia.

Blandford, R. R., and M. H. Wirth, 1973. Automatic array and network detection in the presence of signal variability, SDL-308, Teledyne Geotech, Alexandria, Virginia.

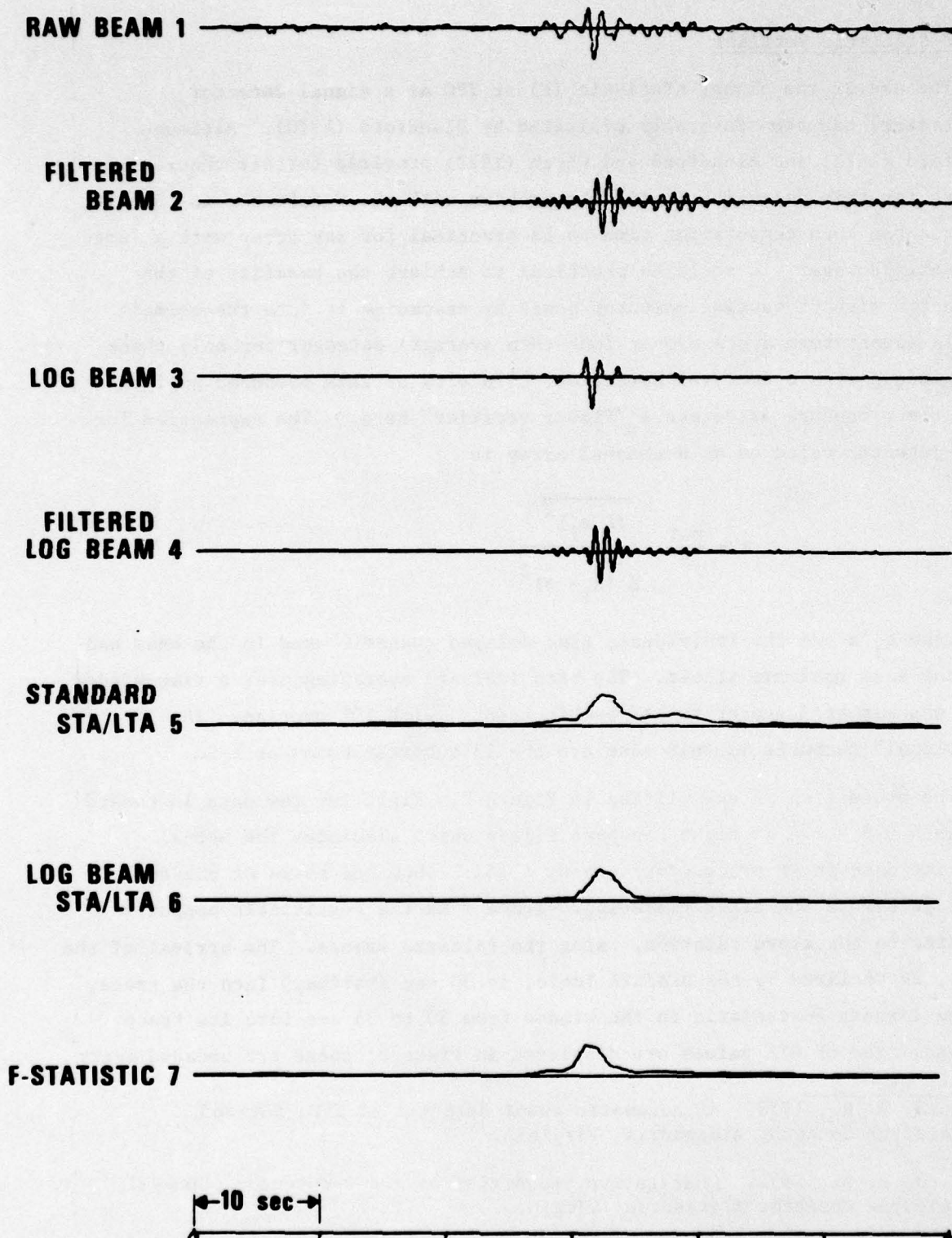


Figure 2. Example of the processing done to test methods for rejecting false alarms from the LASA detection log.

second and they are almost, but not exactly, identical to what is computed in the LASA DP processing. While the STA value used for computing S/N ratio is the maximum of trace 5 in the 30-35 sec window, the corresponding LTA value here is taken from the first 30 seconds of trace regardless of whether another detection occurs within that time, as sometimes happens. (Thus computed S/N ratios here will often be considerably different than original DP ratios and they will often have values below the 14 db limit set by EP on signals.) The maximum F-statistics for the 325 events are plotted versus S/N in Figure 3 with the symbols representing either valid detections (0) or false alarms (x) based upon the categories of Chang et al. Note that these classifications were made prior to the processing described here. A decision line arbitrarily drawn at $F = 5.6$ would correctly identify 86% of the events as false alarms or valid detections. Examination of the 44 events that the Fisher verifier did not correctly classify showed that a majority of the category 1 signals (valid P phases) which had low F-statistics were of very short duration, such that a better performance could be perhaps achieved for the Fisher verifier if the time-averaging window of 2 sec were shortened. Also, some of the supposedly good signals rejected by the Fisher detector had one or more bad channels, which were screened out by the analyst in making his final decision on the detection. Many of the false alarms, which would be passed by the decision line in Figure 3 were signals with a strong, apparently coherent signal which may have been arbitrarily rejected by the analyst. Thus, if a slightly higher level of sophistication were programmed for the Fisher verifier, then the percentage of correct classifications would increase.

Note again that LASA processing presently does not include many of the calculations formerly done in EP. Unphased subarray beams are presently used, with only 0.1 to 0.2 db loss in array threshold. More significantly, no beam correlation or packing is done to improve the DP locations. Thus, the present beam alignments are not optimum and might seriously hamper a Fisher verifier which, by its nature, demands high signal coherency. If the same types of false alarms described above also suffer further degradation in coherence, then a lower F-statistic decision line might still be successful in discriminating valid and invalid detections. However, an experiment, similar to that done here, should be conducted on new data in order to re-evaluate this method.

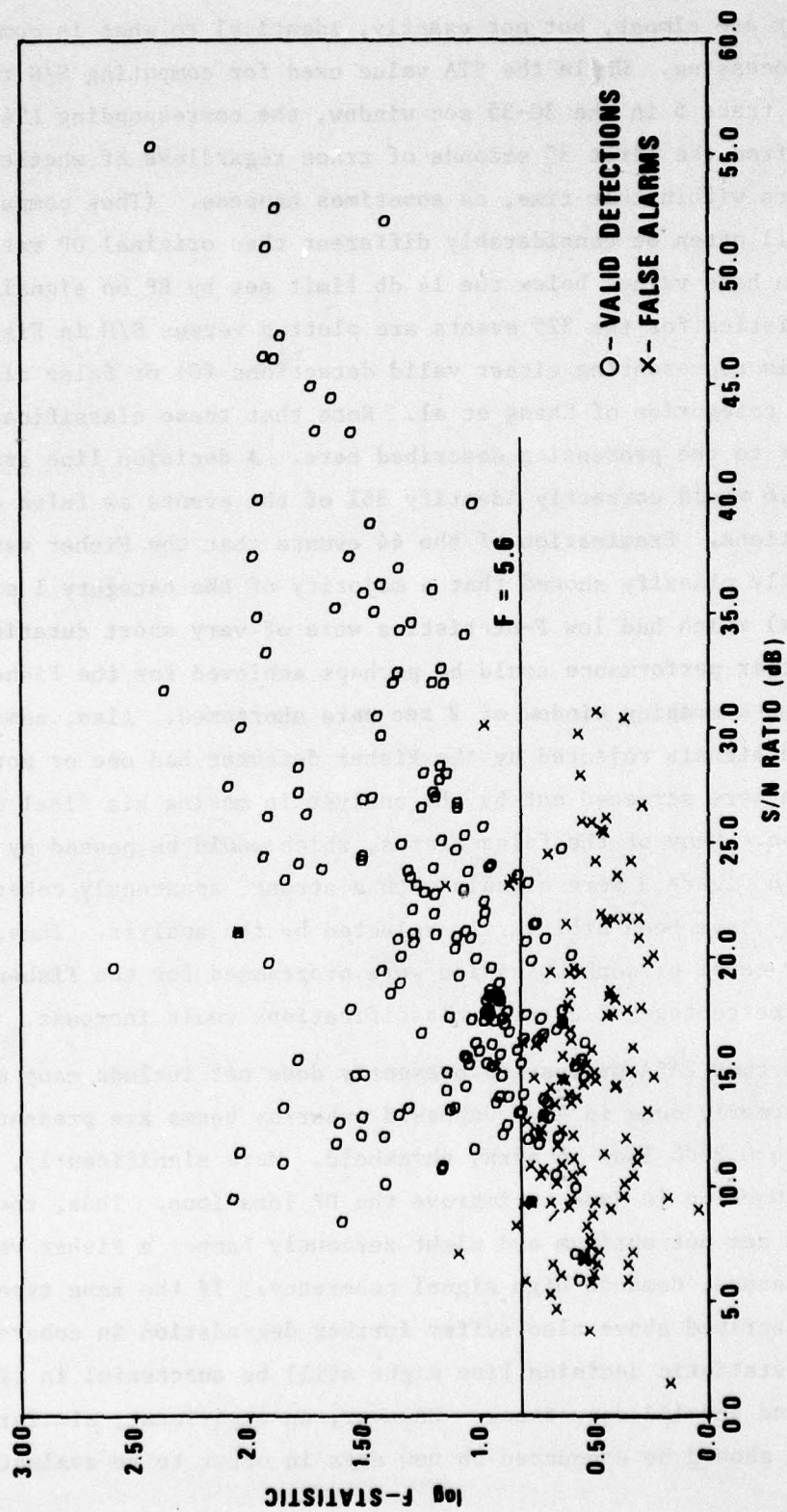


Figure 3. Event classification results for the Fisher verifier.

Logarithmic Beamforming

Weichert and Henger (1976) described the use of log-beaming at the YKA array and showed that this method could successfully reject many false alarms. Muirhead and Datt (1976) discussed a related N-th root beaming process in regard to the WRA array. Both these methods effectively emphasized signal coherency over amplitude alone in making detections and they are very robust in rejecting detections caused by data spikes and related hardware abnormalities. They are more naturally suited to small arrays where signal coherency is high across all the sensors rather than to large arrays such as LASA and NORSAR where signal coherence between widely-spaced sensors may become negligible. Nonetheless, the data base has been processed through a logarithmic beamforming algorithm to determine if it had any potential for discriminating valid and invalid LASA detections. These operations were performed on the appropriately delayed channels

$$s_{ij}^{\ell} = \ln(s_{ij}) \quad \begin{array}{l} i=1, N \text{ subarrays} \\ j=1, M \text{ samples} \end{array}$$

$$s_{.j} = \frac{1}{N} \sum_{i=1}^N s_{ij}^{\ell}$$

$$\hat{s}_{.j} = \exp(|s_{.j}|) \cdot \text{sign}(s_{.j})$$

The resulting values of \hat{s} formed a very unusual representation of seismic data, as exemplified by trace 3 in Figure 2, and were filtered to produce more seismic-like data as in trace 4. An STA series, displayed as trace 6, was computed in the same manner as for the linear beam; and the maximum in the 30-35 second window was used to compute the STA/LTA values. The results are plotted in Figure 4 versus S/N ratio computed from the standard, linear beamforming STA/LTA values. A decision line arbitrarily drawn at $\log(\text{STA/LTA}) = 0.80$ for the log-beaming correctly classifies 75% of the events; this result is not as precise, then, as the Fisher verifier, which achieved an 86% rate. This result, coupled with the fact that no satisfactory theoretical treatment

Muirhead, K. J., and R. Datt, 1976. The N-th root process applied to seismic array data, Geophys. J., 47, 197-210.

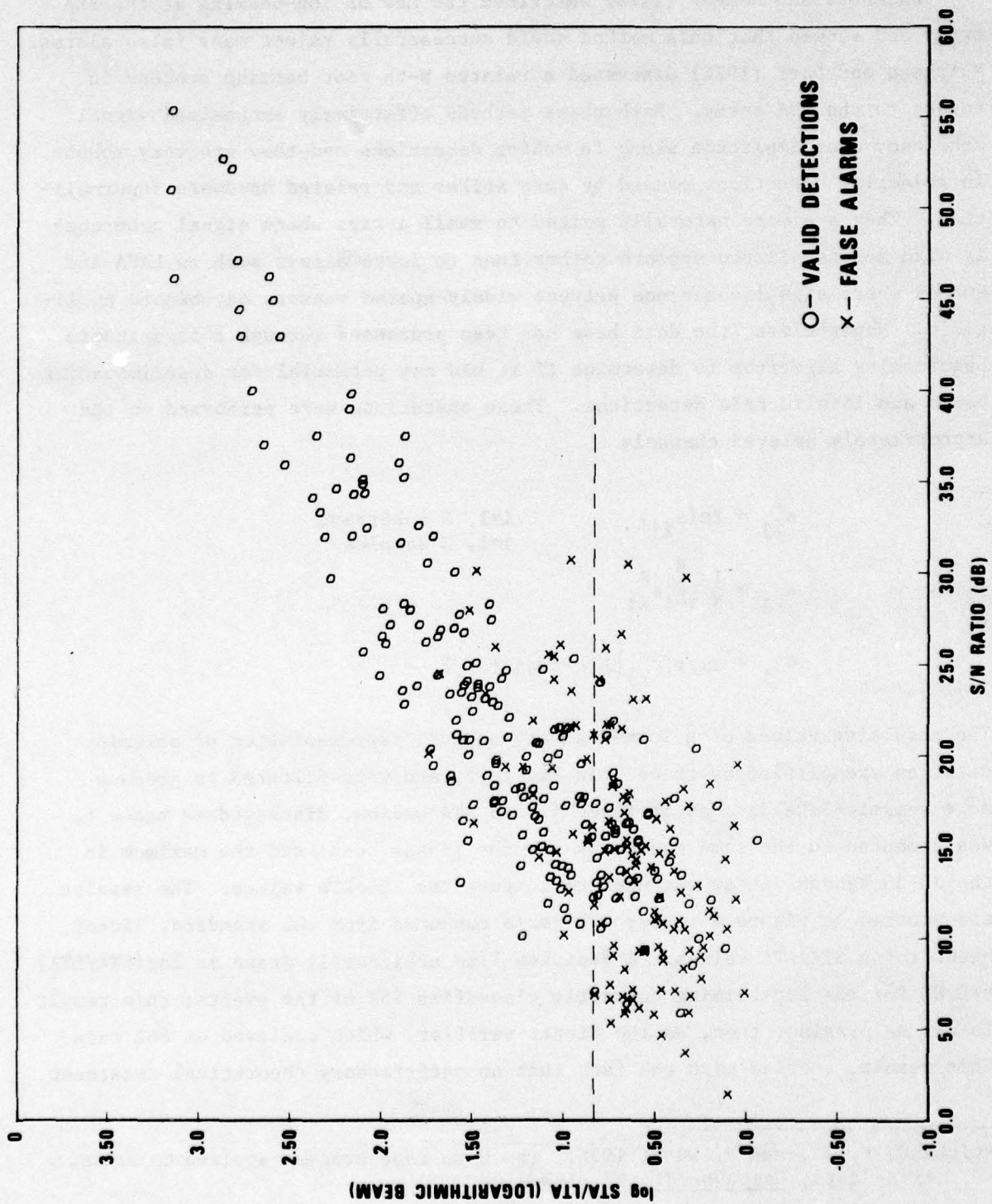


Figure 4. Event classification results for the logarithmic beaming method.

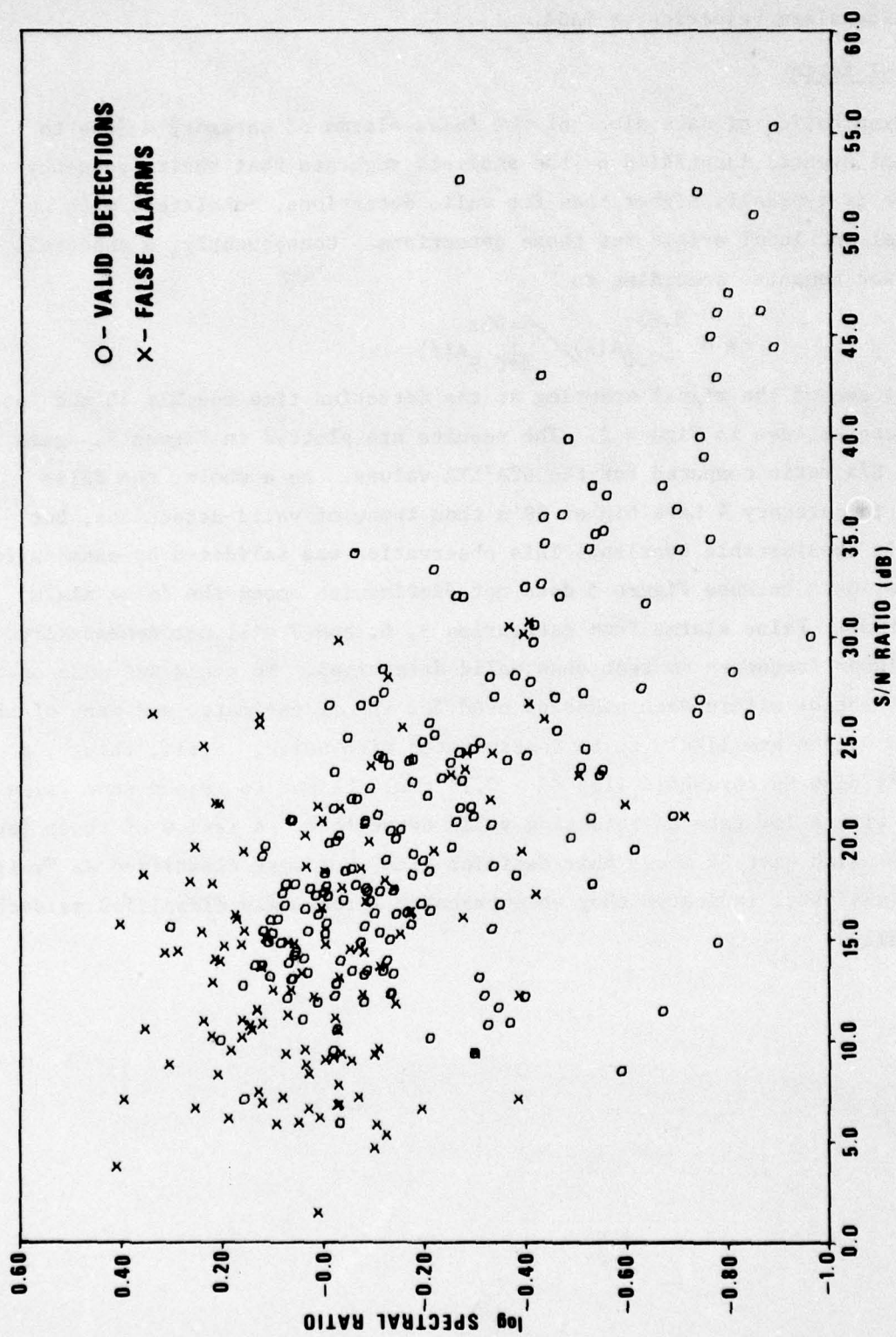


Figure 5. Event classification results for the spectral ratio computation.

exists for log beaming, indicates that this process is not the best strategy for false alarm rejection at LASA.

Spectral Ratio

Examination of data plots of the false alarms of category 4 (due to regional events) identified by the analysts suggests that their frequency content is typically higher than for valid detections, consistent with the regional and local origin for these detections. Consequently, a spectral ratio was computed according to

$$SR = \frac{\sum_{f=2.0}^{3.8\text{hz}} A(f)}{\sum_{f=0.9}^{1.8\text{hz}} A(f)}$$

for 6.4 sec of the signal starting at the detection time roughly 30 sec into the trace as seen in Figure 2. The results are plotted in Figure 5, again versus S/N ratio computed for the STA/LTA values. As a whole, the false alarms in category 4 have higher SR's than those of valid detections, but there is considerable overlap. This observation was validated by examination of print-outs because Figure 5 does not distinguish among the false alarm categories. False alarms from categories 3, 6, and 7 will not necessarily have higher frequency content than valid detections. No check was made on the S/N ratios within each passband used for the SR estimate, and many of the plotted values are likely to be contaminated with noise. Still, though, a suitably high SR threshold (log SR > 0.1) could be set to reject some false alarms with a low rate of rejecting valid detections. A review of those few signals which have SR above this decision line, but were classified as "valid" by the analysts, indicated they were probably erroneously classified as such originally.

P-WAVE ARRIVAL TIMING

LASA EP routinely determined arrival times of events which were processed by comparison with a reference waveform unique to each beam number (Dean and Ahner, 1971). Dean and Ahner's comparison of these automatically determined arrival times with analyst-determined arrival times showed an average absolute error of .25 seconds with roughly a one-second standard deviation for the actual differences. Considerable evidence exists from various illustrations in the seismological literature for sizeable dissimilarity of signals recorded at one site from source regions whose dimensions are only a few wavelengths of 1-Hz P waves, which is a lesser area than what a typical LASA beam represents. Figure 6 is an example of such variability for Kamchatka signals recorded at LASA. Because of the capriciousness of P waveforms, use of a representative event waveform to time arrivals from other events within the same beam area may occasionally lead to large errors. Furthermore, waveform matching is closely linked to the initial detection time declared in LASA DP and it cannot back up on the trace to improve the timing of emergent signals as human analysts are able to do. De Braemacker (1964) investigated a first-motion detector using differencing of data samples, but this approach clearly will be useful only with fairly impulsive arrivals.

As an alternative arrival timing algorithm, the application of a prediction-error (PE) filter to the vertical component has been investigated. Three-component processing would be desirable, but it would be more time-consuming. Also, the author had in mind application of the filter to the VELA array sites and the SRO sites which produce only vertical-component SP recording. Although PE filtering assumes nothing about the signal, it is not a disadvantage because of the random nature of P waveforms. Theoretically, it should detect whenever the time series changes sufficiently in rms level or it is altered in its frequency content. Moltshan et al. (1964) and

De Braemacker, J. C., 1964. Detection of small arrivals, Bull. Seism. Soc. Am., 54, 2141-2164.

Moltshan, G. M., V. F. Pisarenko, and N. A. Smirnova, 1964. Some statistical methods of detecting signals in noise, Geophys. J., 8, 319-323.

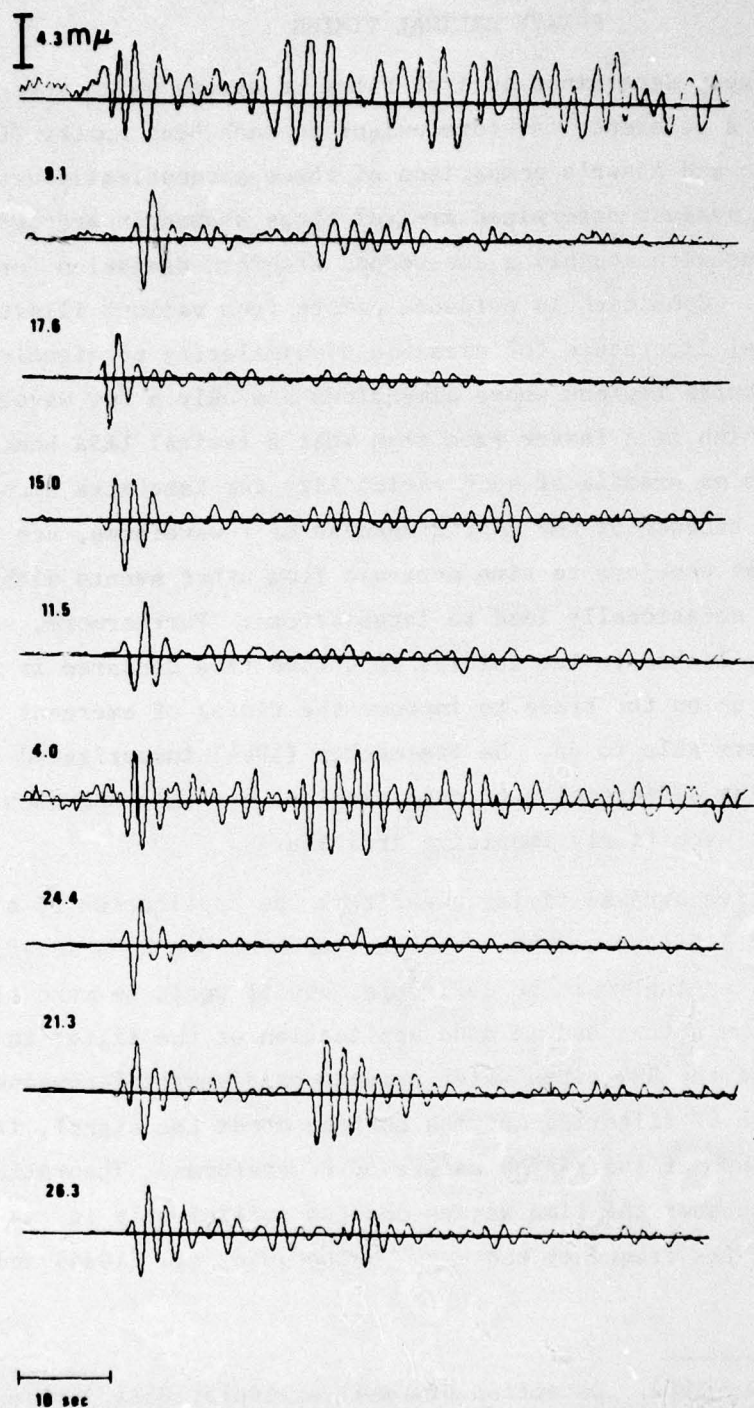


Figure 6. P-wave variability as seen at LASA from a small Kamchatka source region (from Blandford and Clark, 1975).

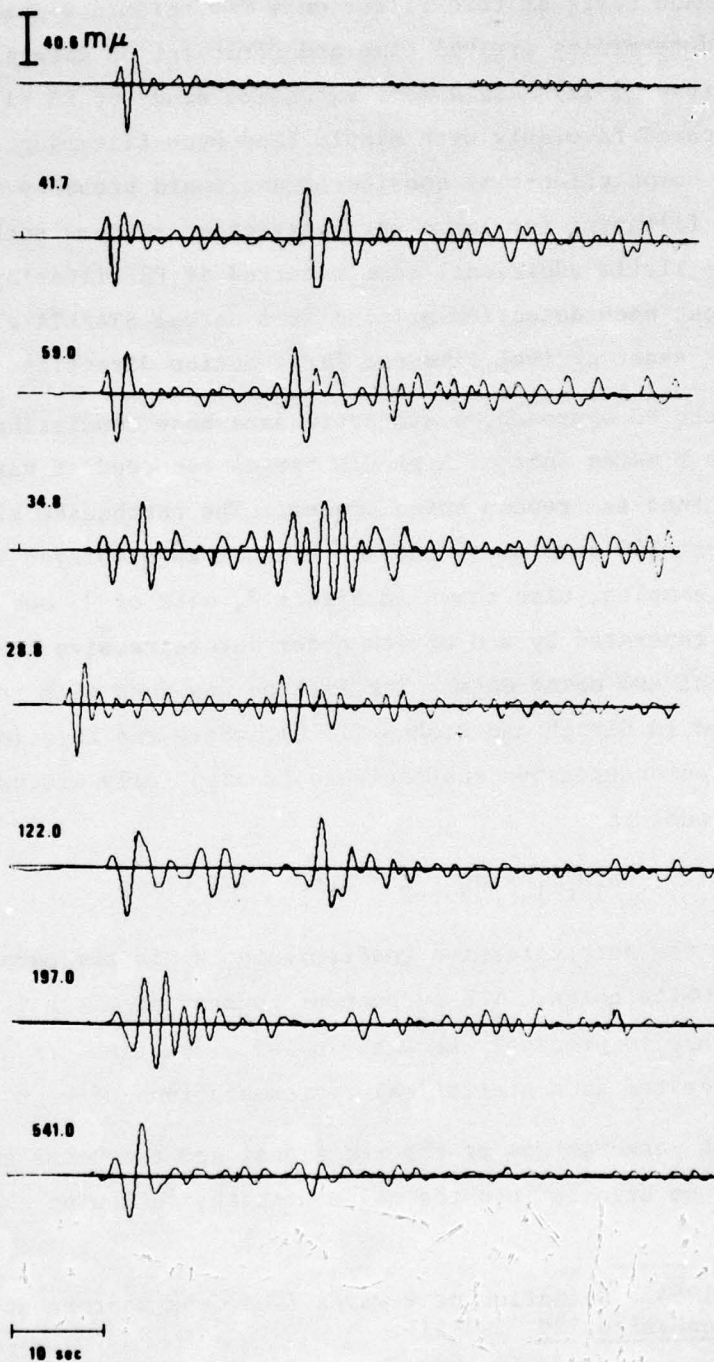


Figure 6 (Cont.). P-wave variability as seen at LASA from a small Kamchatka source region (from Blandford and Clark, 1975).

Claerbout (1964) made tests of this filter on a few seismic signals and found that it aided in determining arrival time and first-motion direction. Gjoystaal and Husebye (1972) made a more extensive study of PE filtering and found that it compared favorably with simple band-pass filtering. Given the present hardware, computation-time considerations would probably rule out the on-line use of PE filtering for large array detection systems such as LASA, but there would be little additional time required if PE filtering were applied to an interval about each detection arising from normal STA/LTA algorithms in order to determine exact arrival time and first-motion direction.

To evaluate the PE approach, a synthetic data base consisting of ten typical earthquake P waves (not of high S/N ratio) recorded at various SRO sites were merged into ten random noise traces. The earthquake signals were limited to the first 100 samples (5 sec) of P onset as displayed in Figure 7. The ten noise samples, also shown in Figure 7, were of 25 sec duration and were artificially generated by use of 4th-order autoregressive models which had been fit to real SRO noise data. The fitting was done with the Yule-Walker algorithm described in Ulrych and Bishop (1975), where the relationship between the PE filter and autoregressive coefficients is also fully discussed. Basically, the noise model is

$$s(t) = a_1 s_{t-1} + a_2 s_{t-2} + a_3 s_{t-3} + \dots + e_t$$

where the a_1 's are the autoregressive coefficients, s_t is the sampled time series, and e_t is white noise. The purpose of generating the noise artificially was to be able to precisely know the noise properties. A different set of a_1 's is generated as a statistical representations of each noise sample.

All 100 of the permutations of the ten signal and ten noise samples were made by inserting the signals into the noise with the following characteristics:

Claerbout, J. F., 1964. Detection of P-waves from weak sources at great distances, Geophysics, 29, 197-211.

Gjoystaal, H., and E. S. Husebye, 1972. A comparison of performance between prediction error and bandpass filters, NORSAR Technical Report No. 48, NTNF/NORSAR, Kjeller, Norway.

Ulrych, T. J., and T. N. Bishop, 1975. Maximum entropy spectral analysis and autoregressive decomposition, Rev. Geophys., 13, 183-200.

P WAVES

NOISE

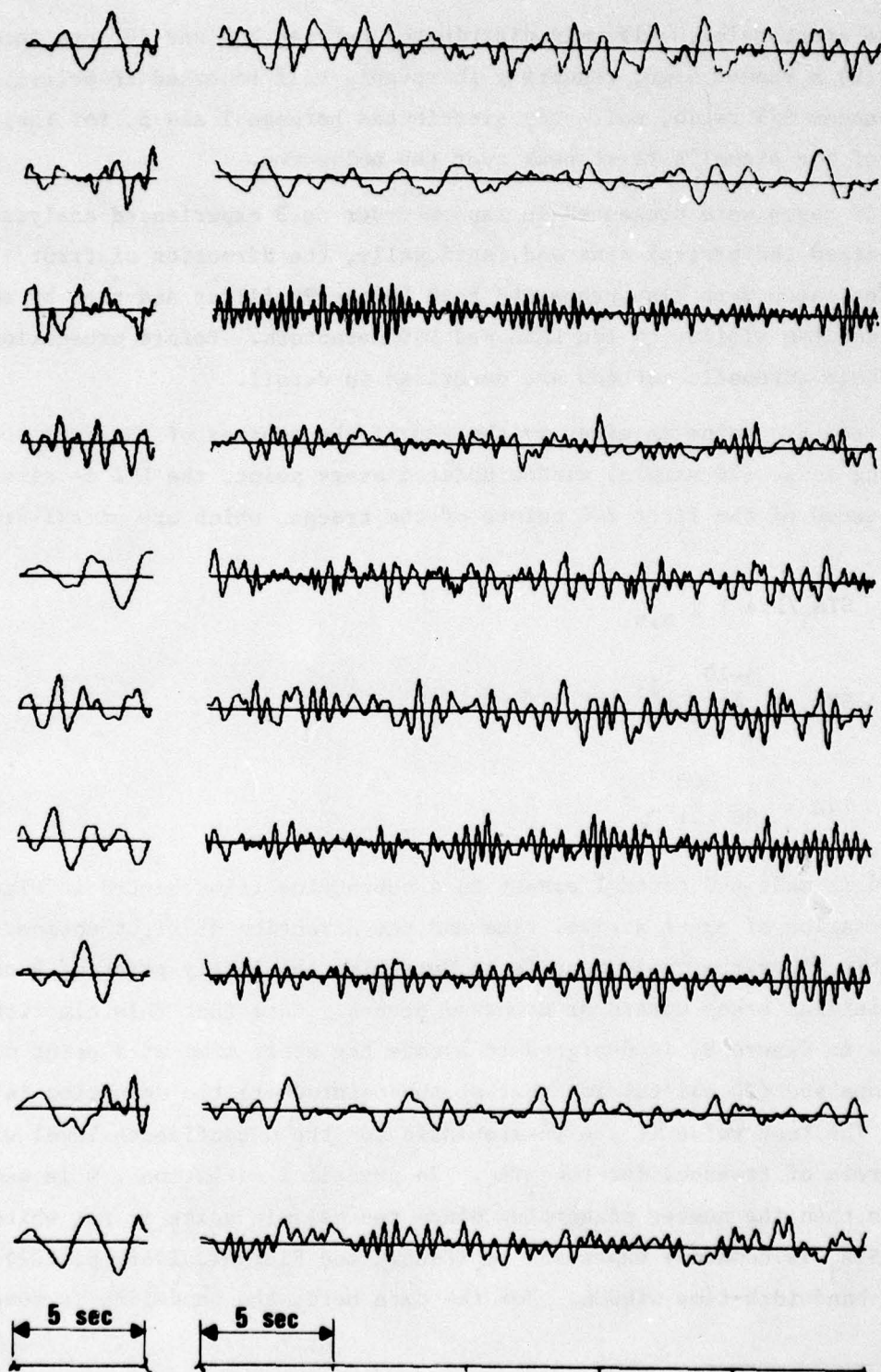


Figure 7. Signals and noise used in the PE evaluation.

1) a random start point, uniformly distributed between 200 and 400 pts into the noise, 2) a random sign, resulting in roughly half reversed in polarity, and 3) a random S/N ratio, uniformly distributed between 1 and 5, for the amplitude of the signal's first peak over the noise rms.

The 100 cases were presented in random order to 3 experienced analysts who then picked the arrival time and, optionally, the direction of first motion. The cases were also processed both by the PE filter and then by an STA/LTA algorithm similar to the LASA and SRO detectors. Before presenting results, these automatic methods are described in detail.

While the STA value is given by the sum of the squares of the data points in a sliding 1-sec (20 sample) window updated every point, the LTA is given by the rms squared of the first 200 points of the traces, which are signal-free. When

$$STA_j / LTA > \chi^2_{\alpha, \nu}$$

where

$$STA_j = \sum_{k=j-9}^{j+10} s_k^2$$

$$LTA = \frac{1}{200} \sum_{k=1}^{200} s_k^2$$

a detection is made and control passes to a subroutine (flowcharted in Figure 8) for determination of exact arrival time and the direction of first motion. The idea this algorithm implements is to determine the likely point of P onset, where the initial break upward or downward occurs. Note that this algorithm, as outlined in Figure 8, is designed to locate the start time at a point no more than one sec (20 points) in front of the point where the detection is declared. The test value is the χ^2 -statistic for the α confidence level with ν DOF (degrees of freedom) for the STA_j . In practical situations, ν is necessarily less than the number of samples since the seismic noise is not white. The ν for STA_j is commonly expressed as (Bendat and Piersol, 1966, p. 202): $\nu(\text{DOF}) = 2 \cdot \text{bandwidth} \cdot \text{time window}$. For the data here, the bandwidth is roughly

Bendat, J. S., and A. G. Piersol, 1966. Measurements and Analysis of Random Data: New York, John Wiley & Sons.

Variables: Y - original trace
 FM - first motion direction
 IS - start point index

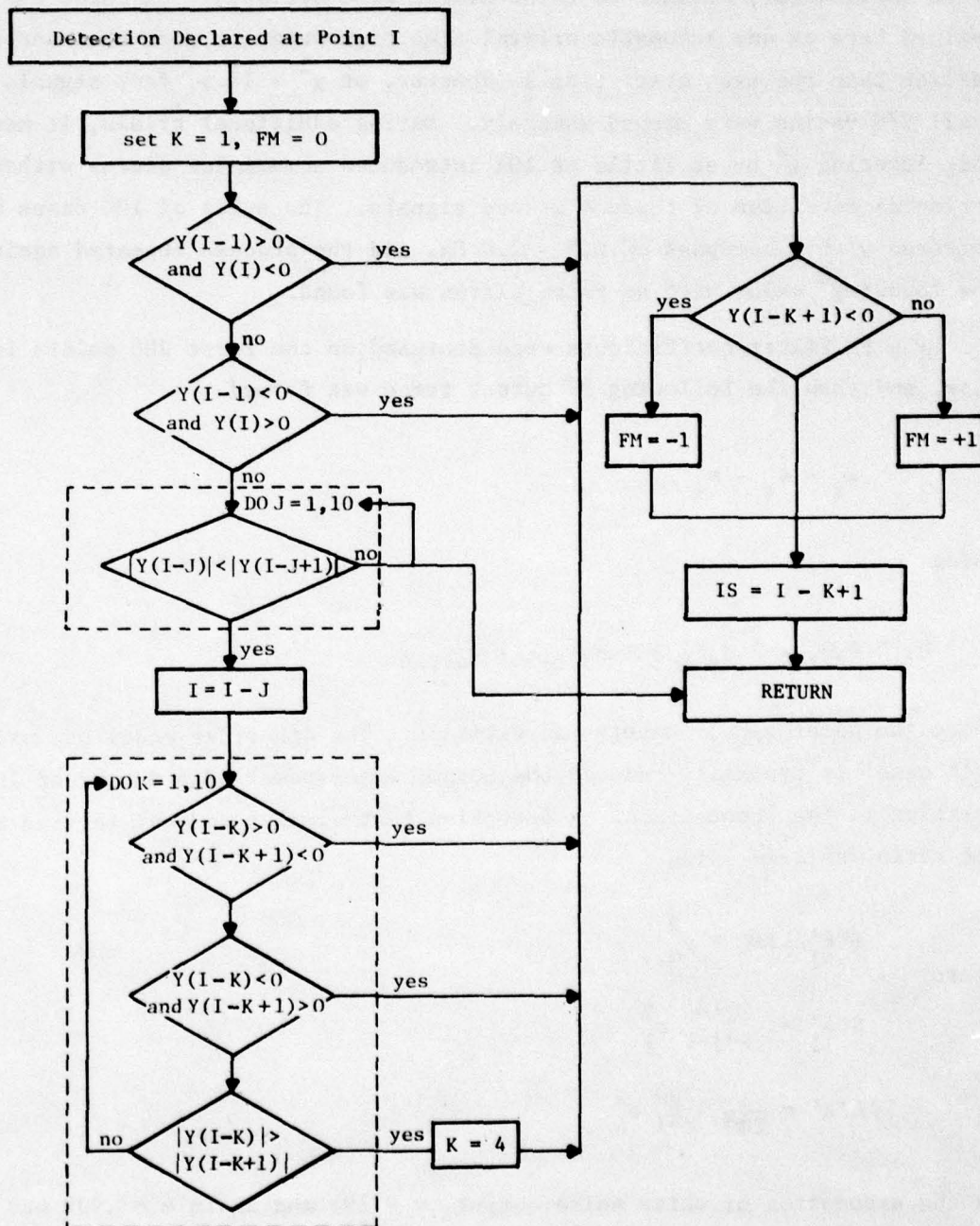


Figure 8. Flowchart of algorithm to pick exact arrival time and first-motion polarity.

37

2 Hz and the time window is 1 sec, giving $\nu \approx 4$. The α point must be chosen quite high to prevent false alarms; we used $\alpha = .999$, giving $\chi^2 \approx 18.5$. This estimate, though only an initial one, when applied to the 100 cases was found to be satisfactory because no false alarms were declared. (A false alarm is defined here as any automatic arrival time pick which is more than one second earlier than the true start time.) However, at $\chi^2 = 18.5$, four signals with small S/N ratios were missed entirely. During additional trials, it was found that lowering χ^2 by as little as 10% introduced some false alarms without achieving detection of those 4 missed signals. The suite of 100 cases was filtered with a bandpass of 0.5 ~ 2.0 Hz, and the process repeated again until the lowest χ^2 value with no false alarms was found.

The PE filter coefficients were designed on the first 200 points in each case, and then the following PE output trace was formed

$$e_t = \hat{s}_t - s_t$$

using

$$\hat{s}_t = \hat{a}_1 s_{t-1} + \hat{a}_2 s_{t-2} + \hat{a}_3 s_{t-3} + \hat{a}_4 s_{t-4}$$

where the caret symbol denotes an estimate. The 4th-order model was used in each case; it typically reduced the output trace power by a factor of 10 relative to the input trace. A detection test similar to that for the STA/LTA ratio was made using

$$\text{where } \text{STA}'_j / \text{LTA}' > \chi^2_{\alpha, \nu}$$

$$\text{STA}'_j = \sum_{k=j-9}^{j+10} e_k^2$$

$$\text{LTA}' = \frac{1}{200} \sum_{k=1}^{200} e_k^2$$

On the assumption of white noise output, $\nu = 19$; and again $\alpha = .999$ was chosen to avoid false alarms. Using these values, $\chi^2 \approx 43.1$. With a threshold set at this level, no false alarms occurred and no detections were missed in the

100 cases. The χ^2 value was reduced until a false alarm appeared, with a final acceptable value set at 38.0 above which no false alarms or missed detections occurred. The exact arrival time and first-motion direction were determined again by entering the algorithm outlined in Figure 8 at the j th point where STA'_j exceeded the χ^2 threshold. Note that this algorithm works on the original data, not the STA_j trace. Applying the PE processor to filtered data did not produce significantly different results over the 100 cases.

The results of applying the basic STA/LTA ratio, with and without filtering, and the PE method are compared to the mean of the three analysts' work in Table I. An example of the time series involved in both the STA/LTA and PE processing is shown in Figure 9. Table I indicates that the PE processing is superior to the STA/LTA method for determining arrival time on the basis of these results only. However, in a practical sense, some weight must be given to the simplicity of the STA/LTA method. Also the missing signals that occur using the simple STA/LTA method are not a real problem since they involved lower S/N ratio than the LASA, NORSAR, or SRO detection systems operationally pass. Table I shows that the PE processing is roughly equivalent to human analysts in the ability to determine start time and first-motion polarity. Recall that the analysts performed their determinations on unfiltered data; and, although some improvement might be expected with the benefit of a filter, the results of the simple STA/LTA method applied to filtered traces was not significantly different. This suggests that such improvement might not be realized by the analysis either.

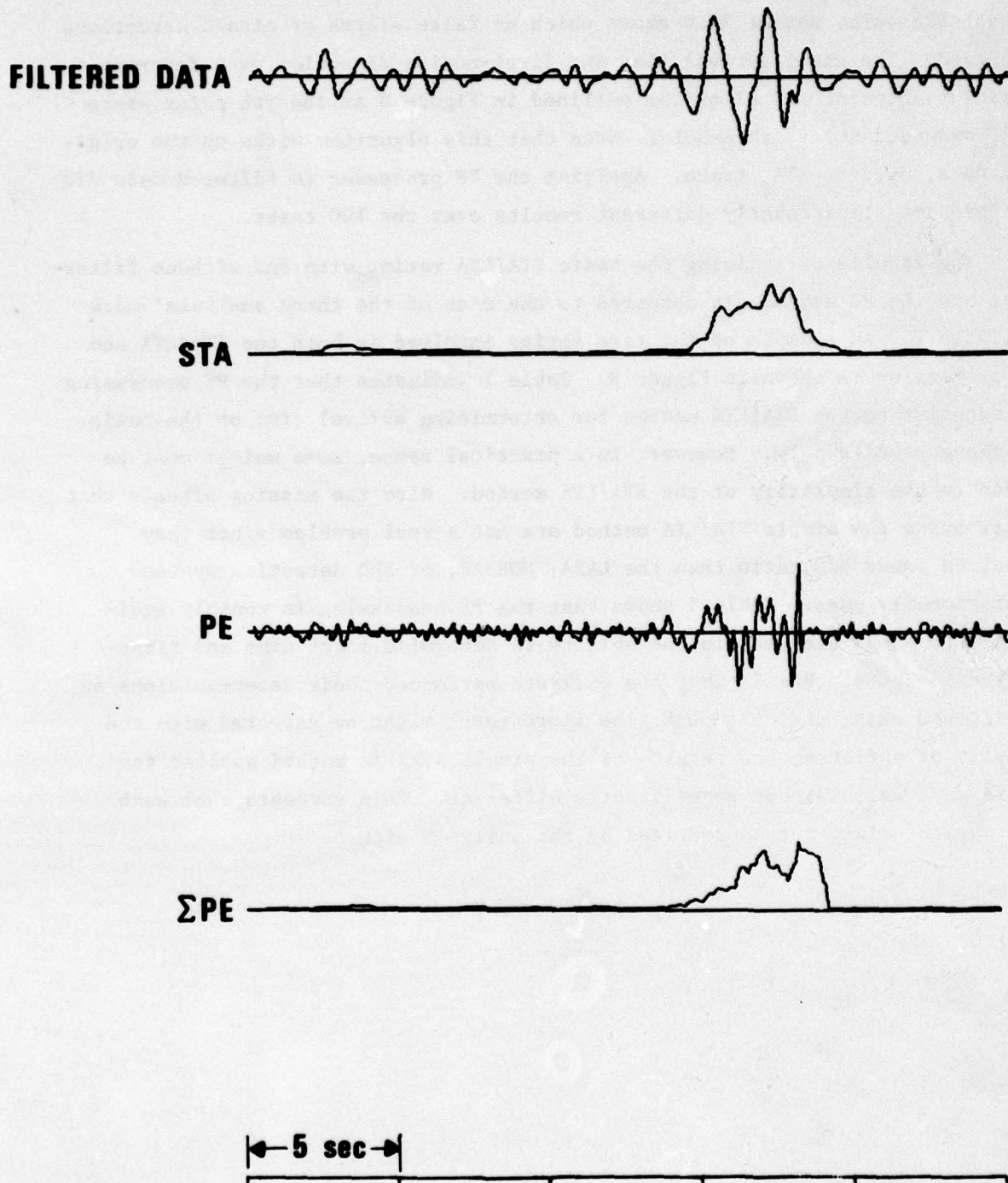


Figure 9. Example of the start-time determination by STA/LTA and PE algorithms.

TABLE I

Accuracy of P Arrival Time and First-Motion Determination
by Automated Means Versus Human Analysts

<u>Mode of Determining Start Time</u>	<u>No.** False Alarms</u>	<u>No.*** Missed</u>	<u>Mean Absolute Error (sec)</u>	<u>% of First Motion Correct</u>
STA/LTA	0	4	.65	71%
filter + STA/LTA	0	2	.65	65%
PE filtering	0	0	.45	81%
human analyst*	1.7	0	.43	77%****

* results averaged over three analysts

** false alarm is declared if pick is more than 1 sec. early

*** missed detection declared if pick is more than 5 sec. late

**** analysts did not report first motion direction in all cases

LR-WAVE ARRIVAL TIMING

For Rayleigh waves, neither a simple STA/LTA algorithm nor a PE filter will be satisfactory for determining the arrival time because of the dispersed nature of such arrivals. If the epicenters are known, a method described by Massé (1975) can provide arrival-time predictions based on approximate ray-tracing over a global group-velocity grid. The accuracy of the predictions is limited in this case only by our knowledge of the earth's structure and the chosen size of the grid elements. The author made extensive use of such a grid program for purposes of visual analysis of HGLP seismograms (von Seggern, 1976). The maximum errors in such predictions were found to be 5 minutes for the largest epicentral distances. Somewhat more precise timing is required if automated magnitude estimation is to be combined with the detection of LR waves.

A technique presented by Smart (1977) can simultaneously determine the time window of maximum S/N ratio for given frequencies and estimate the spectral amplitude as a function of frequency. The reliability of the results is assessed in terms of an F-statistic measure of signal presence in reference to a coherent Love-Rayleigh model of ground motion. Smart's processor, although robust in continuous-time processing of LP data for detection purposes, could serve a more limited role of signal "verifier" and "timer" when applied to broad windows selected on the basis of arrival-time predictions from a group-velocity grid such as mentioned above. The processor operates in the spectral domain, after transformation of a portion of the time series, with the time-window length a variable. Details can be found in Smart (1977), but essentially a least-squares solution for the Love-Rayleigh signal components (vertical, radial, and transverse) in several frequency bands is obtained from the raw 3-component data (Z, N, and E), including an estimate of the arrival azimuth. These components are then rotated back into Z', N', and E'

Massé, R. P., 1975. A technique for computing surface-wave properties, Bull. Seism. Soc. Am., 65, 1743-1751.

von Seggern, D. H., 1976. Final report on the analysis of recordings from the Very Long Period Stations, SDAC-TR-76-1, Teledyne Geotech, Alexandria, Virginia.

Smart, E., 1977. A 3-component, single-station, maximum-likelihood surface-wave detector, SDAC-TR-77-14, Teledyne Geotech, Alexandria, Virginia.

seismograms; and the F-statistic given by

$$F = \frac{\Sigma(Z'^2 + N'^2 + E'^2)}{\Sigma[(Z-Z')^2 + (N-N')^2 + (E-E')^2]}$$

where the sums are taken over Fourier components, is computed as an indicator of the S/N value. High values of the statistic, especially across several frequency bands, are interpreted as verification of Rayleigh-Love signal presence, provided the computed azimuth agrees reasonably with the expected one.

It is appropriate here to emphasize the advantages of Smart's processor over other long-period processing methods for detection, such as bandpass filtering, polarization filtering (Simons, 1968; Choy and McCamy, 1973), match filtering (Capon et al., 1969), and adaptive processing (Barnard and O'Brien, 1974):

- 1) no assumption need be made about the arrival azimuth;
- 2) only linear processes are performed, so true signal amplitude information is relatively well preserved;
- 3) it is extremely fast; in demonstrations it ran 100 times real time on an IBM 360/44 for a 3-component site (Smart, 1977);
- 4) a statistical confidence measure of signal presence is provided;
- 5) false-alarm rates can be estimated from noise properties.

The other processors each have some, but not all, of these desirable properties.

Simons, R., 1968. PHILTRE-A surface wave particle motion discrimination process, Bull. Seism. Soc. Am., 58, 629-637.

Choy, G., and K. McCamy, 1973. Enhancement of long-period signals by time varying adaptive filters, J. Geophys. Res., 78, 3505-3511.

Capon, J., R. J. Greenfield, and R. T. Lacoss, 1969. Long period signal processing results for the Large Aperture Seismic Array, Geophysics, 34, 305-329.

Barnard, T. E., and L. J. O'Brien, 1974. An evaluation of adaptive-beamforming techniques applied to seismic data, ALEX(01)-TR-74-08, Texas Instruments, Inc., Dallas, Texas.

An example of the use of the processor is shown in Figure 10 which illustrates the rotated Z, R, and T traces (rotated with respect to the expected great-circle azimuth.) Here the basic window length was 256 sec with computations performed on successive, 25% overlapping windows of the raw Z, N, and E traces. The window with the maximum F-statistic (provided $F > 14.0$) for the band about $T = 20$ sec period ($.040 \leq f \leq .055$) is marked, along with the deviation of the computed azimuth from the expected great circle azimuth. These windows are good approximations to what a human analyst would set as the arrival window of 20-sec LR waves. Note that for some stations, with evident LR signals, no detection was declared by the automatic process. The lack of detection was due either to data irregularities in some cases or to the signal's poor S/N ratio in the 25 to 18 second band in others. This process then selects the best window, based upon the F-statistic, for computation of Rayleigh-wave magnitudes, according to a manner described in a later section of this report.

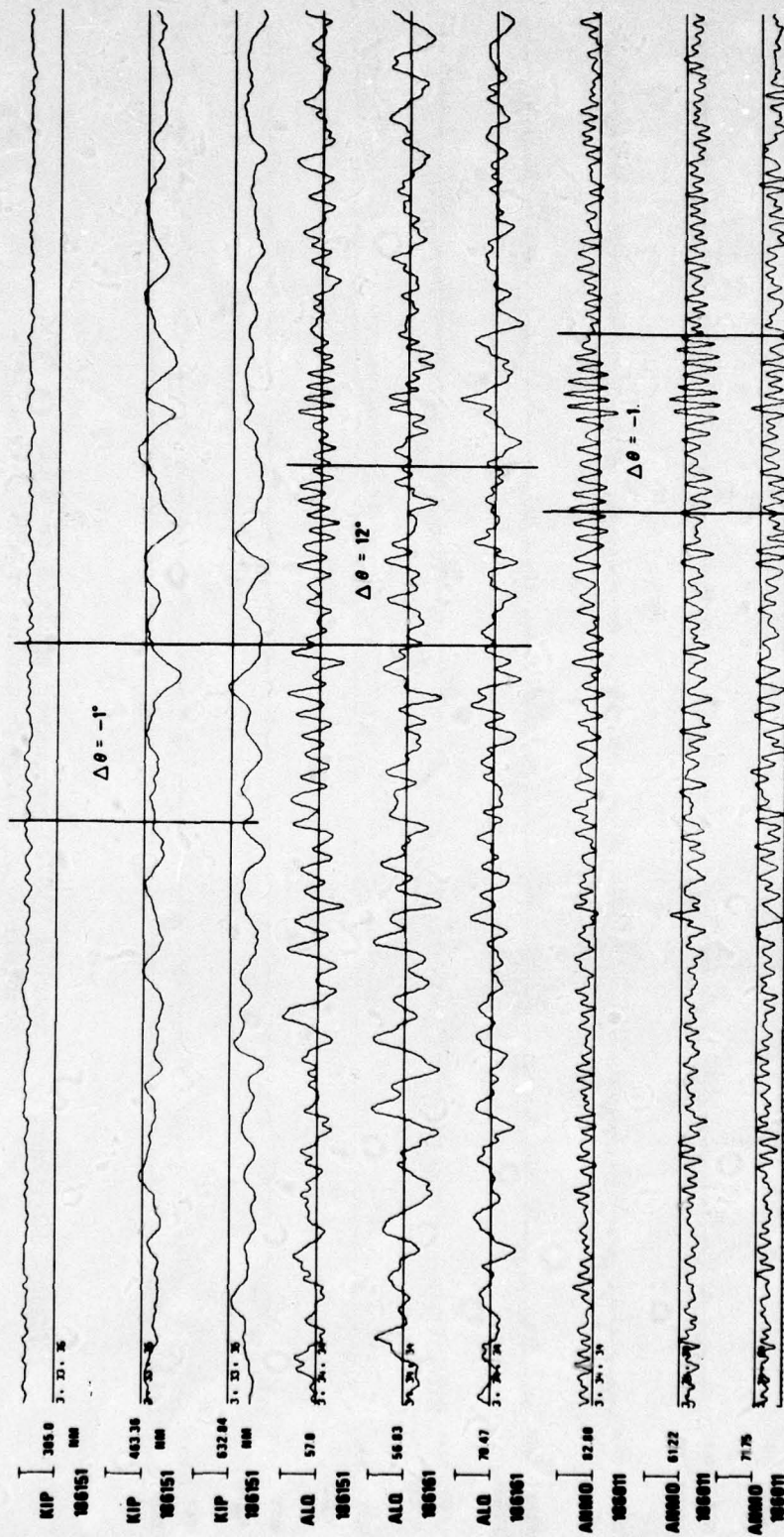


Figure 10. Smart's (1977) processor applied to HGLP and SRO recordings of a Kazakh explosion (04 July 1976).

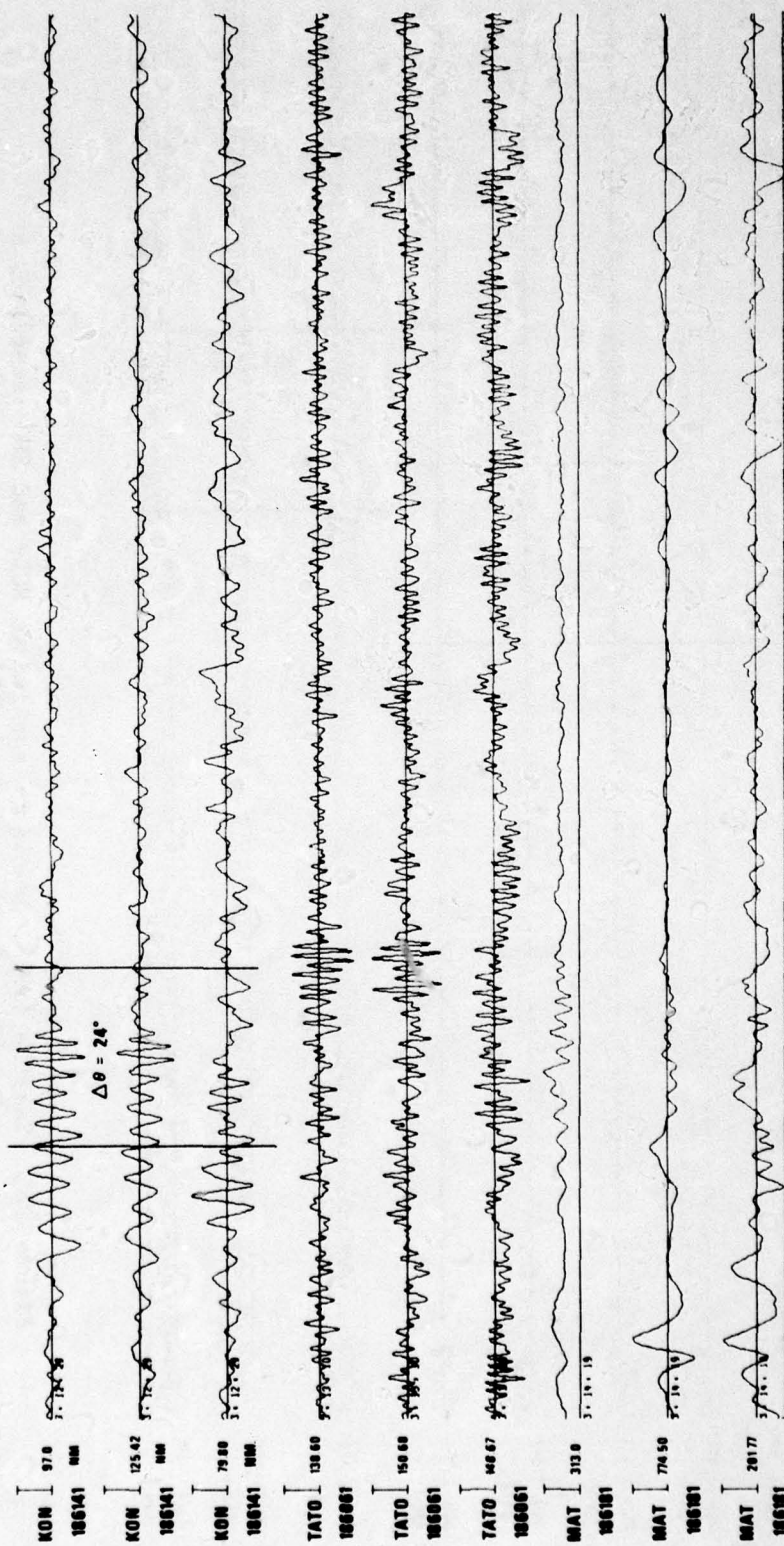


Figure 10 (Cont.). Smart's (1977) processor applied to HGLP and SRO recordings of a Kazakh explosion (04 July 1976).

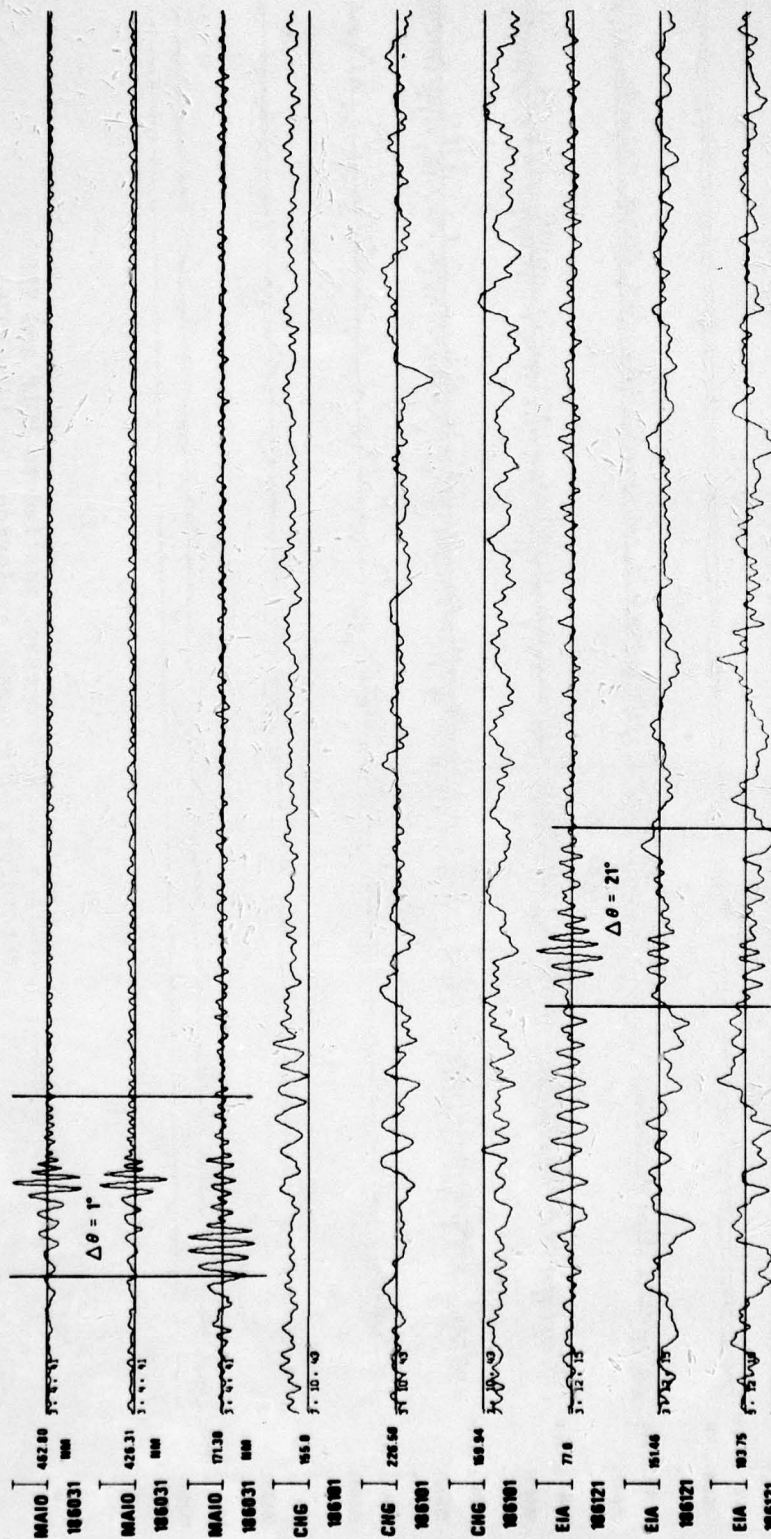


Figure 10 (Cont.). Smart's (1977) processor applied to HGLP and SRO recordings of a Kazakh explosion (04 July 1976).

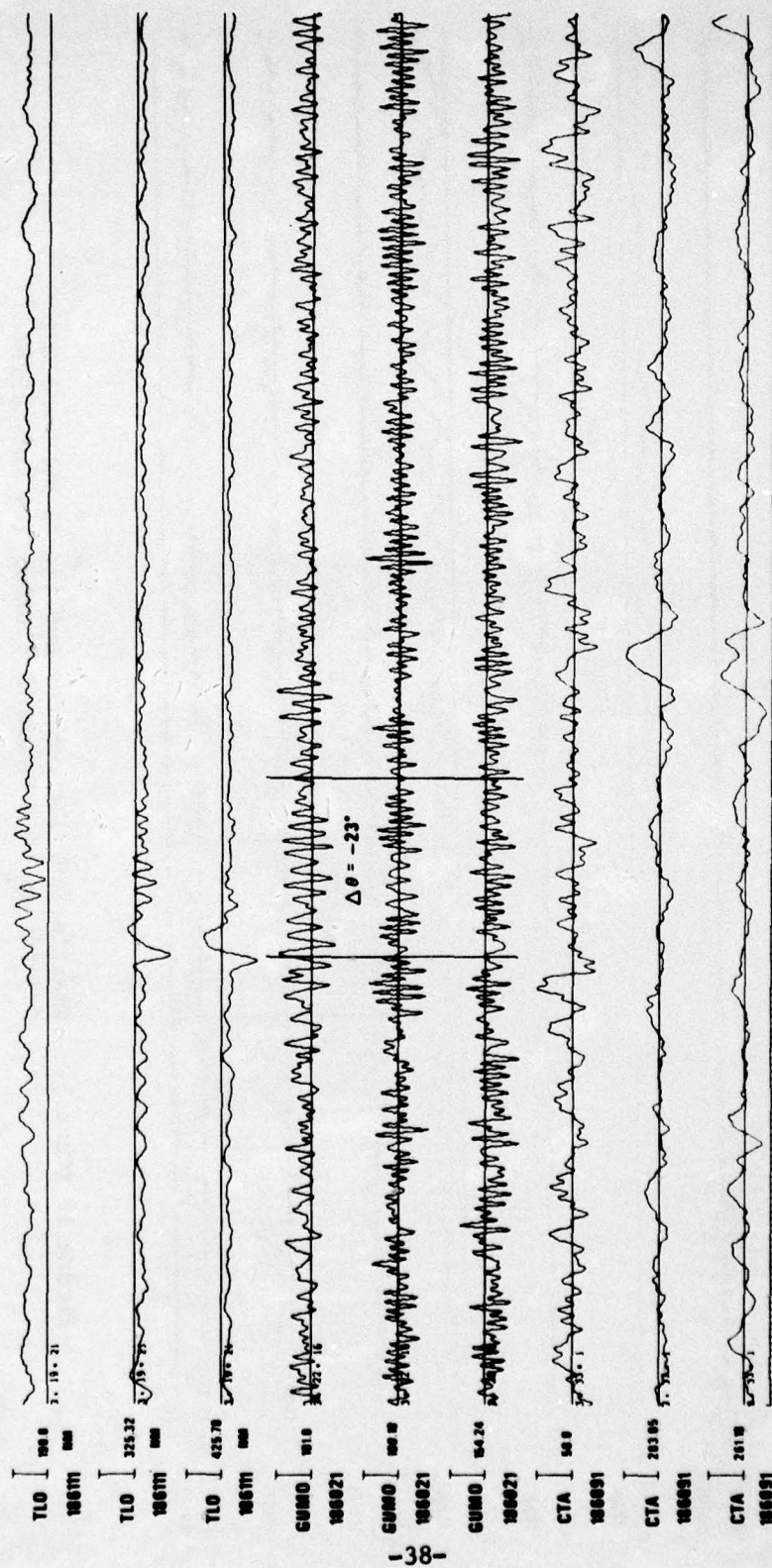


Figure 10 (Cont.). Smart's (1977) processor applied to HGLP and SRO recordings of a Kazakh explosion (04 July 1976).

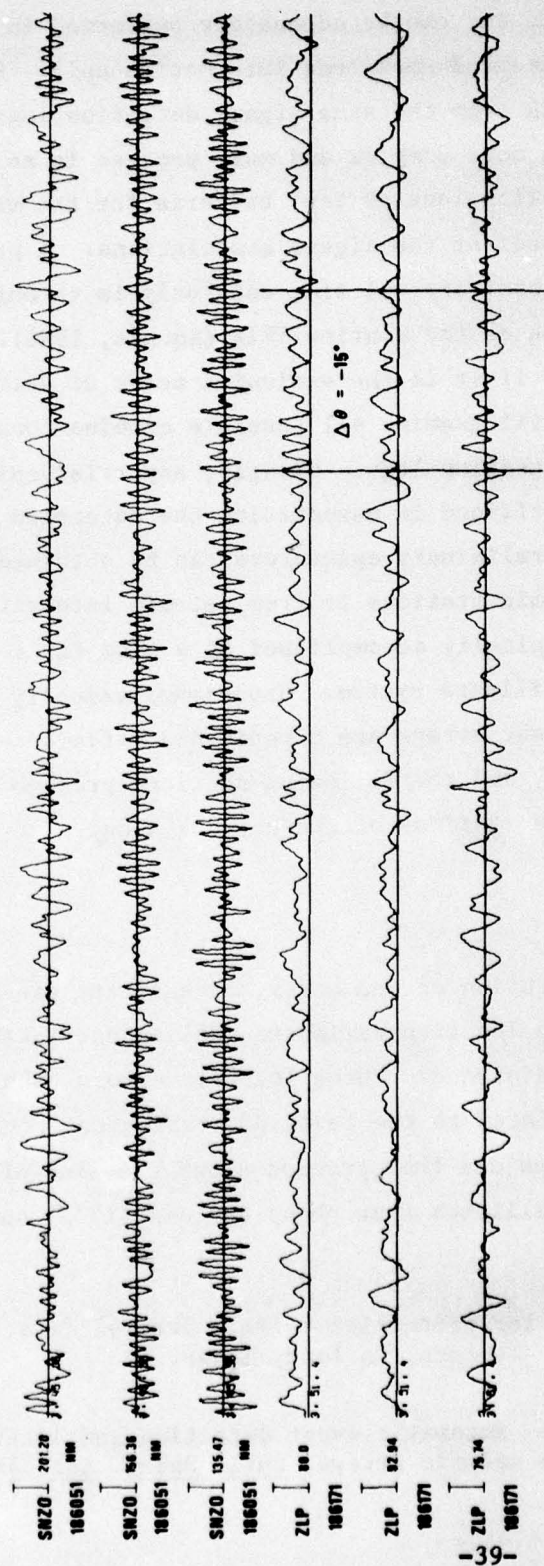


Figure 10 (Cont.). Smart's (1977) processor applied to HGLP and SRO recordings of a Kazakh explosion (04 July 1976).

AUTOMATIC ASSOCIATION

The task of associating reported seismic arrivals to known events is fairly straightforward in principle and can be adequately performed in practice on the basis of travel-time and amplitude information only. However, if the task of inferring the events from the same signal detection logs is included, the process becomes much more complex and must proceed in an iterative manner with numerous applications of test criteria for the validity of epicenters and for the correctness of the signal associations. A proven method of inferring events from global arrival-time data only is through a three-station search procedure such as the routine TRIX (Kovacs, 1966). This process can be very time-consuming if it is the exclusive means of determining trial epicenters though since it will examine all possible combinations of three station arrivals from the detection logs. Clearly, any trial epicenters established beforehand should be utilized in associating the detection data from the various stations. Such preliminary epicenters can be obtained from regional or local networks of seismic stations or from seismic intensity reports. However, such data gathering is typically accomplished at a pace far too slow for a near-real-time seismic surveillance system. The signal velocity and azimuth estimates produced by seismic arrays are a rapid and efficient means of obtaining trial epicenters, though, and the following sections presume the availability of such data from some stations of the network along with ordinary single-sensor detection logs.

Associating Array Locations

Based on the size and configuration of the array, an estimate can be made of the accuracy of the array's location estimates (Shlien and Toksöz, 1973) as a function of epicentral distance. These location errors take the form of ellipses, whose size is related to the level of statistical confidence. Association of array-detected phases can then proceed along the line of testing the overlapping of the confidence ellipses that Shoup and Sax (1975) outlined.

Kovacs, P., 1966. LOCAS, a system for processing seismic arrival data (U), Report No. TR-66-103, Teledyne Geotech, Garland, Texas, (Classified).

Shlien, S., and M. N. Toksöz, 1973. Automatic event detection and location capabilities of large aperture seismic arrays, Bull. Seism. Soc. Am., 63, 1275-1288.

Note that their procedure is based upon the important assumption that correct phase identification has been made and, therefore, that an array detection maps into one and only one location. Experience with LASA at the SDAC and, in fact, the whole of global seismic recording indicates that sufficient later phases are detected so that assumption of P (or PKP) alone for a detected signal is often incorrect. Shlien and Toksöz (1974) dealt with this complication by testing with computations nearly all hypotheses on phase types, given the observed $dT/d\Delta$'s and arrival times at two arrays (LASA and NORSAR), and then selecting the best pair of arrival identifications, with the corresponding location. (The "best" pair is defined by the highest of the likelihood ratios resulting from values of each of the hypotheses over the value of a null hypothesis of random arrivals.) Their results demonstrated that a significant number of later arrivals were in the detection logs and could lead to successful associations.

While Shlien and Toksöz (1974) concluded that such a phase identifier for two arrays could operate easily within real time, the authors needed to estimate the efficiency for M arrays. A basic and efficient unit of time to consider is one hour of detection logs. Let the number of hourly detections from each array log be N; then by the Shlien and Toksöz algorithm, the number of likelihood ratio tests for two arrays is given by

$$L_2 = \frac{N!K}{2!(N-2)!}$$

where K is the number of hypotheses tested for each pair from the two detection logs ($K = 49$ in Shlien and Toksöz). If M arrays contribute detection logs, all possible pairs of arrays must be considered for each of the L_2 tests so that

$$L_M = \frac{N!K}{2!(N-2)!} \frac{M!}{2!(M-2)!}$$

Some hypothetical, though reasonable, numbers can be used for evaluation of this expression. Letting $N = 10$ detections per hour from each array, $M = 5$ arrays, and $K = 49$ hypotheses, 22,000 tests would need to be performed per

Shlien, S. and M. N. Toksöz, 1974. Automatic phase identification with one and two large aperture seismic arrays, Bull. Seism. Soc. Am., 64, 221-234.

hour of recording time. This figure does not seem prohibitive considering the small extent of the computations required for each likelihood ratio test. Also, some savings are achieved because associated detections are then removed from further consideration. However, this system is also a disadvantage because first acceptable associations are made, not best associations.

The likelihood-ratio test that Shlien and Toksöz (1974) suggested involved distribution functions for the event parameters (latitude, longitude, origin time, and magnitude) fit to data from an extensive past recording period for each array. Seismic bulletins produced for the arrays served to define a training set of beam estimates that could be compared to refined (NEIS) estimates of these parameters. In future expansions of the VELA network, such data will not be immediately available; therefore, a more non-parametric procedure of associating array locations is discussed.

The procedure examined here is the clustering approach to the grouping of data vectors (Williams and Lance, 1977). The data vector from each array would again be the event parameters: latitude, longitude, origin time, and magnitude. Again, multiple hypotheses must be made as to the identity of each phase in the detection log. The clustering algorithm will then compute the Euclidian distance, defined below, between event vectors and group those detections with nearly identical vectors.

First, an estimate of the number of the test distances to be computed and compared will be made. Suppose again that $N = 10$ detections per hour per array and $M = 5$ arrays. Let the variable number J of phase interpretations for each detection, dependent on $dT/d\Delta$, average 5; then the number of event parameter vectors given by $M \times N \times J$ equals 250 per hour of seismic recording. Since the cluster algorithm will examine the proximity of all pairs of these vectors then

$$L = \frac{(M \cdot N \cdot J)!}{2!(M \cdot N \cdot J - 2)!}$$

Williams, W. T., and G. N. Lance, 1977. Hierarchical classificatory methods, in Statistical Methods for Digital Computers, ed. K. Enslien et al.: New York, John Wiley & Sons.

gives the number of repetitions of the basic test, roughly 31,000 in this case. Again, this figure does not seem prohibitive. (Actually, the clustering algorithm proceeds iteratively, defining one new cluster in each step and averaging the associated vectors to produce a new data vector to be compared to the others; but the above estimate of the test is a good approximation.) The clustering can be terminated at any desired level of the proximity test; otherwise all event vectors would be associated finally. One advantage of the clustering approach is that all hypotheses for a given detection are available, and the best hypothesis should ordinarily be selected if more than one association is possible for a given detection.

A test data base for clustering was taken from the detection logs of LASA, NORSAR, and YKA for the time frame 03:19 to 06:53 (origin time) on 19 February 1977. A total of 91 detections were present. From the NEP bulletin, five earthquakes were known to be present in this time frame. For this test, only the P(PKP) phase interpretation was permitted for each detection, and the amplitude was not used as a variable in the event vector. A 4-dimensional event vector was composed of the following:

$$p_1 = \theta/\pi$$

$$p_2 = \frac{1}{2} \cdot \cos\phi \cdot \sin\theta$$

$$p_3 = \frac{1}{2} \cdot \sin\phi \cdot \sin\theta$$

$$p_4 = 15 \cdot \frac{OT - OT_1}{OT_2 - OT_1}$$

where θ and ϕ are the colatitude and east longitude in radians, OT is the array-estimated origin time of the event converted to seconds, and OT_1 and OT_2 are the first and last origin-time estimates from the array detections (03:19 and 06:53 in this case), converted to seconds. The parameter p_4 is weighted such that an origin-time difference of roughly 12 sec is nearly equal to one degree of epicentral difference from p_1 . The vector or Euclidean difference between event pairs is computed to serve as the test points for clustering in the program, a version of BMDP2M. The program was allowed to proceed through all 90 steps; in each step one new cluster was

formed by association of one of the 91 detections to a previous cluster and the data amalgamated to generate a new cluster event vector. The output, in the form termed a dendogram, is shown in Figure 11. The lower levels of the dendogram are not shown here. At the highest levels, associations of multiple detections are formed from an array for one event. The clustering steps at which detections from four of the five known events were amalgamated are indicated by circles. LASA and NORSAR were not associated for one NEP event because the LASA detection was of a core phase, with a consequent poor array location. Note also the two associations made at high level and designated by rectangles; these are apparent events not found on the NEP bulletin. No attempt has been made in this study to determine an optimum value for cutting off associations when proceeding down the dendogram.

Both clustering and maximum-likelihood hypothesis testing would be suitable for the task of simultaneously associating detections and forming events from a multiple-array network. However, at least two flaws can be seen in both these procedures: 1) they overcompute by testing all possibilities, most of which are of such low probability of association that they seldom need to be considered; 2) they fail to take account of and to utilize those few good detections from each array among the many lesser quality or nearly useless detections; 3) these procedures do not accommodate data from single-sensor sites, which have no event parameter estimates but still contribute heavily to the final NEP bulletin; 4) they do not include a method of refining the epicenters by the classically proven least-squares location method, which is required when associating four or more first arrivals.

NEP Automatic Association

In devising the automatic association (AA) algorithm at the SDAC, a more efficient and variable strategy was sought that could be tailored to a changing and growing network composed of arrays and single sites. The roots of the procedure are found in the ADAPS set of algorithms (Geotech, 1968), although the utilization of large-array data such as from LASA or NORSAR is new. The basic

Geotech, 1968. ADAPS, an automatic data association and processing system for seismological data, Volume 3, Program descriptions, TR-68-28, Teledyne Geotech, Garland, Texas.

procedure is flowcharted in Figure 12. The overriding principle governing this strategy is to make use of the best data first to initiate associations, leading to event locations. The automated strategy is not unlike what a human analyst would do, given a composite detection list from arrays and single-sensor sites of varying capability. The details of the AA algorithm can be found in the NEP documentation, and here we give only a simplified description.

The reason for the outermost DO loop in Figure 12 is to use primarily P-wave detections ($\Delta < 100^\circ$) first in defining an array-estimated trial epicenter to which other arrivals will be associated. The only other phases which arrive with velocities of the direct P are S and PP with their surface reflections and pP; since these will rarely be detected without an accompanying prior P detection, the likelihood of initiating automatic association from trial epicenters projected by arrays from these arrivals on the false assumption of a direct P arrival is small. Only after all data association possibilities are exhausted using P arrivals will the algorithm attempt to use the higher velocity arrivals ($d\Delta/dT > 25$ km/sec) which are characteristically less easily identified and which produce locations of much less accuracy due to their high velocity, even if correctly identified. The second DO loop in Figure 12 orders the signals by decreasing signal/noise ratio limits, again insuring that the best signals are used first. The third DO loop orders the arrays by the assumed accuracy of their beam locations. The highest priority array ALK is composed of a central site and four "outriggers," for a total aperture of roughly 400 km. A special ALK algorithm estimates a velocity and azimuth on the assumption of a plane-wave arrival over at least three of the five separate stations. The innermost DO loop in Figure 12 then searches the detection list over the appropriate time frame (up to 22 minutes after the estimated event origin time) for detections whose arrival time (also $dT/d\Delta$ and velocity estimates if an array) fits the trial epicenter to within one minute on the assumption that it is a P or PKP detection. If four or more arrivals are thus associated, an attempt is made to refine the trial location with HYPO, a standard least-squares location algorithm. Various checks are applied until a satisfactory group of stations is used to define a hypocenter or until it is determined that the presumed event cannot be located. In the former case, the associated arrivals are removed from further consideration

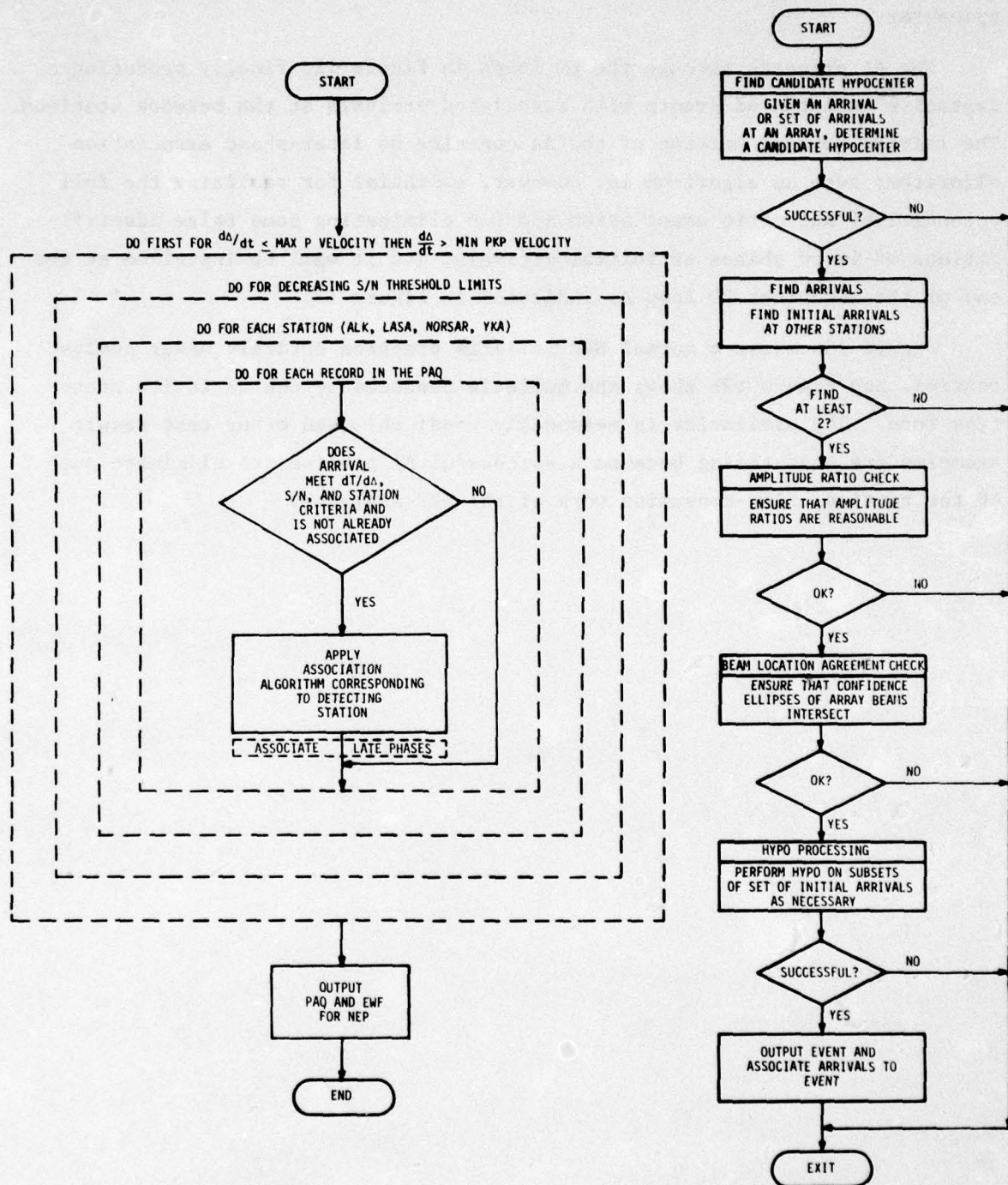


Figure 12. Basic flowchart of the automatic association program used for preparing the NEP bulletin.

in AA while in the latter they are free to be associated with a new trial epicenter.

The AA proceeds through the DO loops in Figure 12, finally producing a tentative bulletin of events with associated arrivals at the network stations. The initial working version of the AA contains no later-phase association algorithm; such an algorithm is, however, essential for realizing the full potential of automatic association and for eliminating some false identifications of later phases as initial arrivals, and it will be installed at the end of the innermost DO loop as indicated in Figure 12.

Figure 13a shows a normal NEP bulletin prepared entirely under analyst control, and Figure 13b shows the bulletin produced by the AA in its prototype form. The similarity is reasonably good; this and other test result examples are encouraging because a successful AA promises to eliminate much of the routine, time-consuming work of the NEP analysts.

SUMMARY OF SDAC VELA NETWORK REPORT LOCATIONS-----AUTOMATIC ASSOCIATION
DATA DATE 2 JAN 72 ()

2		3	9	28.4	52.8N 158.0E	OKN	218	NEAR EAST COAST OF KAMCHATKA	
4	THAK	1	18	57.0	D	-1.0	21.8	267.7	88.8
4	PCAK	1	18	57.0	D	-1.0	21.8	267.6	88.7
4	CHAK	1	18	57.0	D	-1.0	21.8	267.6	88.8
4	WJAK	1	18	57.0	D	-1.0	21.8	267.7	88.7
4	THAK	1	16	17.0	D	-1.3	17.8	270.2	37.3
4	WRC	1	16	17.0	D	-1.3	17.8	270.2	37.3
4	YKA	1	17	17.0	D	-1.3	17.8	270.2	37.3
4	LA	1	17	17.0	D	-1.3	17.8	270.2	37.3
2		3	11	23.1	59.8N 167.0E 489KM	OKN	A77	EASTERN SIBERIA	
4	THAK	1	18	57.0	D	-1.1	17.8	276.4	61.2
4	PCAK	1	18	57.0	D	-1.1	17.8	276.4	61.2
4	CHAK	1	18	57.0	D	-1.1	17.8	276.4	61.2
4	WJAK	1	18	57.0	D	-1.1	17.8	276.4	61.2
4	THAK	1	16	17.0	D	-1.1	17.8	276.4	61.2
4	WRC	1	16	17.0	D	-1.1	17.8	276.4	61.2
4	YKA	1	17	17.0	D	-1.1	17.8	276.4	61.2
4	LA	1	17	17.0	D	-1.1	17.8	276.4	61.2
2		3	30	40.7	64.1N 135.1W	OKN	A77	NORTHWEST YUKON TERRITORY, CANADA	
4	THAK	1	30	40.7	D	-1.0	21.8	267.7	88.8
4	PCAK	1	30	40.7	D	-1.0	21.8	267.7	88.8
4	CHAK	1	30	40.7	D	-1.0	21.8	267.7	88.8
4	WJAK	1	30	40.7	D	-1.0	21.8	267.7	88.8
4	THAK	1	34	20.2	D	-1.0	21.8	267.7	88.8
4	WRC	1	34	20.2	D	-1.0	21.8	267.7	88.8
4	YKA	1	32	0.0	D	-1.0	21.8	267.7	88.8
4	LA	1	30	11.0	D	-1.0	21.8	267.7	88.8
2		7	07	26.2	45.7N 74.4E 224KM	OKN	358	KAMCHATKA	
4	THAK	1	07	26.2	D	-1.0	21.8	267.7	88.8
4	PCAK	1	07	26.2	D	-1.0	21.8	267.7	88.8
4	CHAK	1	07	26.2	D	-1.0	21.8	267.7	88.8
4	WJAK	1	07	26.2	D	-1.0	21.8	267.7	88.8
4	THAK	1	06	40.7	D	-1.0	21.8	267.7	88.8
4	WRC	1	06	40.7	D	-1.0	21.8	267.7	88.8
4	YKA	1	07	26.2	D	-1.0	21.8	267.7	88.8
4	LA	1	07	26.2	D	-1.0	21.8	267.7	88.8
2		8	20	16.1	20.4N 174.7E	OKN	234	EAST CHINA SEA	
4	THAK	1	20	16.1	D	-1.0	21.8	267.7	88.8
4	PCAK	1	20	16.1	D	-1.0	21.8	267.7	88.8
4	CHAK	1	20	16.1	D	-1.0	21.8	267.7	88.8
4	WJAK	1	20	16.1	D	-1.0	21.8	267.7	88.8
4	THAK	1	06	40.7	D	-1.0	21.8	267.7	88.8
4	WRC	1	06	40.7	D	-1.0	21.8	267.7	88.8
4	YKA	1	08	40.7	D	-1.0	21.8	267.7	88.8
4	LA	1	02	16.7	D	-1.0	21.8	267.7	88.8
2		10	50	20.8	37.7S 60.1W	OKN	184	ANTARCTICA	
4	THAK	1	50	20.8	D	-1.0	21.8	267.7	88.8
4	PCAK	1	50	20.8	D	-1.0	21.8	267.7	88.8
4	CHAK	1	50	20.8	D	-1.0	21.8	267.7	88.8
4	WJAK	1	50	20.8	D	-1.0	21.8	267.7	88.8
4	THAK	1	50	20.8	D	-1.0	21.8	267.7	88.8
4	WRC	1	50	20.8	D	-1.0	21.8	267.7	88.8
4	YKA	1	50	20.8	D	-1.0	21.8	267.7	88.8
4	LA	1	50	20.8	D	-1.0	21.8	267.7	88.8
2		10	51	1.6	31.3S 69.0W	OKN	127	SAN JOAN PROVINCE, ARGENTINA	
4	THAK	1	51	1.6	D	-1.0	21.8	267.7	88.8
4	PCAK	1	51	1.6	D	-1.0	21.8	267.7	88.8
4	CHAK	1	51	1.6	D	-1.0	21.8	267.7	88.8
4	WJAK	1	51	1.6	D	-1.0	21.8	267.7	88.8
4	THAK	1	51	1.6	D	-1.0	21.8	267.7	88.8
4	WRC	1	51	1.6	D	-1.0	21.8	267.7	88.8
4	YKA	1	51	1.6	D	-1.0	21.8	267.7	88.8
4	LA	1	51	1.6	D	-1.0	21.8	267.7	88.8
2		13	6	58.0	15.4S 165.1E	OKN	184	NEW HEBRIDES ISLANDS	
4	THAK	1	10	27.3	D	-1.2	42.2	216.6	19.3
4	PCAK	1	10	27.3	D	-1.2	42.2	216.6	19.3
4	CHAK	1	10	27.3	D	-1.2	42.2	216.6	19.3
4	WJAK	1	10	27.3	D	-1.2	42.2	216.6	19.3
4	THAK	1	10	27.3	D	-1.2	42.2	216.6	19.3
4	WRC	1	10	27.3	D	-1.2	42.2	216.6	19.3
4	YKA	1	10	27.3	D	-1.2	42.2	216.6	19.3
4	LA	1	10	27.3	D	-1.2	42.2	216.6	19.3
2		23	6	25.7	18.0W 91.5W	OKN	70	GUATEMALA	
4	THAK	1	13	18.3	D	-1.2	18.3	168.4	167.0
4	PCAK	1	13	18.3	D	-1.2	18.3	168.4	167.0
4	CHAK	1	13	18.3	D	-1.2	18.3	168.4	167.0
4	WJAK	1	13	18.3	D	-1.2	18.3	168.4	167.0
4	THAK	1	13	18.3	D	-1.2	18.3	168.4	167.0
4	WRC	1	13	18.3	D	-1.2	18.3	168.4	167.0
4	YKA	1	13	18.3	D	-1.2	18.3	168.4	167.0
4	LA	1	13	18.3	D	-1.2	18.3	168.4	167.0
2		23	6	40.8	16.6W 93.7W	OKN	62	NEXT TO GUATEMALA BORDER REGION	
4	THAK	1	13	18.3	D	-1.2	18.3	168.4	167.0
4	PCAK	1	13	18.3	D	-1.2	18.3	168.4	167.0
4	CHAK	1	13	18.3	D	-1.2	18.3	168.4	167.0
4	WJAK	1	13	18.3	D	-1.2	18.3	168.4	167.0
4	THAK	1	13	18.3	D	-1.2	18.3	168.4	167.0
4	WRC	1	13	18.3	D	-1.2	18.3	168.4	167.0
4	YKA	1	13	18.3	D	-1.2	18.3	168.4	167.0
4	LA	1	13	18.3	D	-1.2	18.3	168.4	167.0
2		23	12	58.1	50.1N 121.1W	OKN	23	NORTH COLUMBIA	
4	THAK	1	13	18.3	D	-1.2	18.3	168.4	167.0
4	PCAK	1	13	18.3	D	-1.2	18.3	168.4	167.0
4	CHAK	1	13	18.3	D	-1.2	18.3	168.4	167.0

Figure 13b. NEP bulletin formed by an automatic association program.

DEPTH ESTIMATION

Depth control on hypocenter solutions in a global seismic bulletin is typically poor. Often, earthquakes as deep as 100 km or more may be constrained to the surface - or a "normal" crustal depth - and surface focus events may be located well below the crust. The classic example is the Long Shot explosion in the Aleutian arc which was located 70 km deep using the Herrin (1968) travel-time tables and over 300 arrival times (Lambert et al., 1969). Lomnitz (1977) correctly emphasizes the non-orthogonality of origin time and depth in hypocenter solutions when reporting stations are only teleseismic. Considerable improvement in depth accuracy can be obtained when stations at regional distance report arrival times, but all too often such data is lacking. Another useful technique is the use of master or reference event observations to remove the travel-time bias associated with the path to each station. Evernden (1969) claims that shallow hypocenters in Kamchatka located in this manner are within roughly 30 km of the true depth with 95% confidence. Blandford (1975) discusses the depth indeterminacy for weak shallow events and demonstrated with NTS explosion times that poorly recorded (5-9 stations) explosions could, with significant probability, be located relatively deeply (up to 100 km). From this he inferred that shallow or crustal earthquakes in the same area could not be reliably discriminated on the basis of hypocenter estimates, even with master event times.

The delay time of the pP phase, if it can be reliably identified, effectively constrains the earthquake depth to within a few km. The degree of errors depend upon the deviation of the true structure in the epicentral

Lambert, D. G., D. H. von Seggern, S. S. Alexander, and G. A. Galat, 1969. The Long Shot experiment, Volume II, Comprehensive analysis, SDL-234, Teledyne Geotech, Alexandria, Virginia.

Lomnitz, C., 1977. A procedure for eliminating the indeterminacy in focal depth determinations, Bull. Seism. Soc. Am., v. 67, 533-535.

Evernden, J., 1969. Identification of earthquakes and explosions by use of teleseismic data, J. Geophys. Res., 74, 3828-3856.

Blandford, R. R., 1975. Use of source-region-station time corrections at NTS for depth estimation, SDAC-TR-75-4, Teledyne Geotech, Alexandria, Virginia.

region from the assumed one, which is usually taken to be uniform over the globe, and the accuracy of the arrival time determinations for pP. However, identification of pP is a seismic analysis decision which, in many cases, is vexatious and unreliable. Clearly, the availability of multi-station data helps to eliminate spurious phases at individual stations and settle upon a suite of pP choices that indicate a common event depth from all or most stations. The following presentation is of an automated scheme to perform this multi-station enhancement of the pP, designed to complement an analyst's judgement.

Method of Automating pP Depth Determination

Figure 14 presents the schematic of a program for automatically determining depth on the basis of pP detection over a network of stations. A fuller description of the process is presented here.

Short-period vertical recordings from M stations of a network are initially aligned on the arrival times of the P-waves. Only stations in the range $10^\circ < \Delta < 100^\circ$ are used. The algorithm then proceeds to form and test hypotheses on the correct depth of focus by shifting and beaming the network of stations according to the appropriate pP times at each station for the given depth hypothesis. Before beaming, the individual channels are subjected to the following steps: 1) are filtered between 0.5 and 2.2 Hz with a tight bandpass filter; 2) have their mean values removed; 3) are rectified by squaring the amplitudes of the sample points; 4) are smoothed with a flat three-second summation window and; 5) have all points divided by the mean square noise value σ^2 , as described next.

Since the ultimate decision on the presence of pP over the entire network will be based on the strength of the beamed signal in the pP window, a comparison window of noise must be selected and entered in the computation of statistical confidence. This window may vary from station-to-station and is first chosen by the following criteria: 1) it is between the P and pP and 2) it is at least 10 seconds long, but not within 10 sec of the P arrival time and 5 sec of the presumed pP arrival time. If such a window does not exist, it is then allowed to shrink to 5 sec. If this change still does not permit a noise window between P and pP, then a window is selected 10 sec

VARIABLES: K depths to be tested
M stations
N points in smoothing window

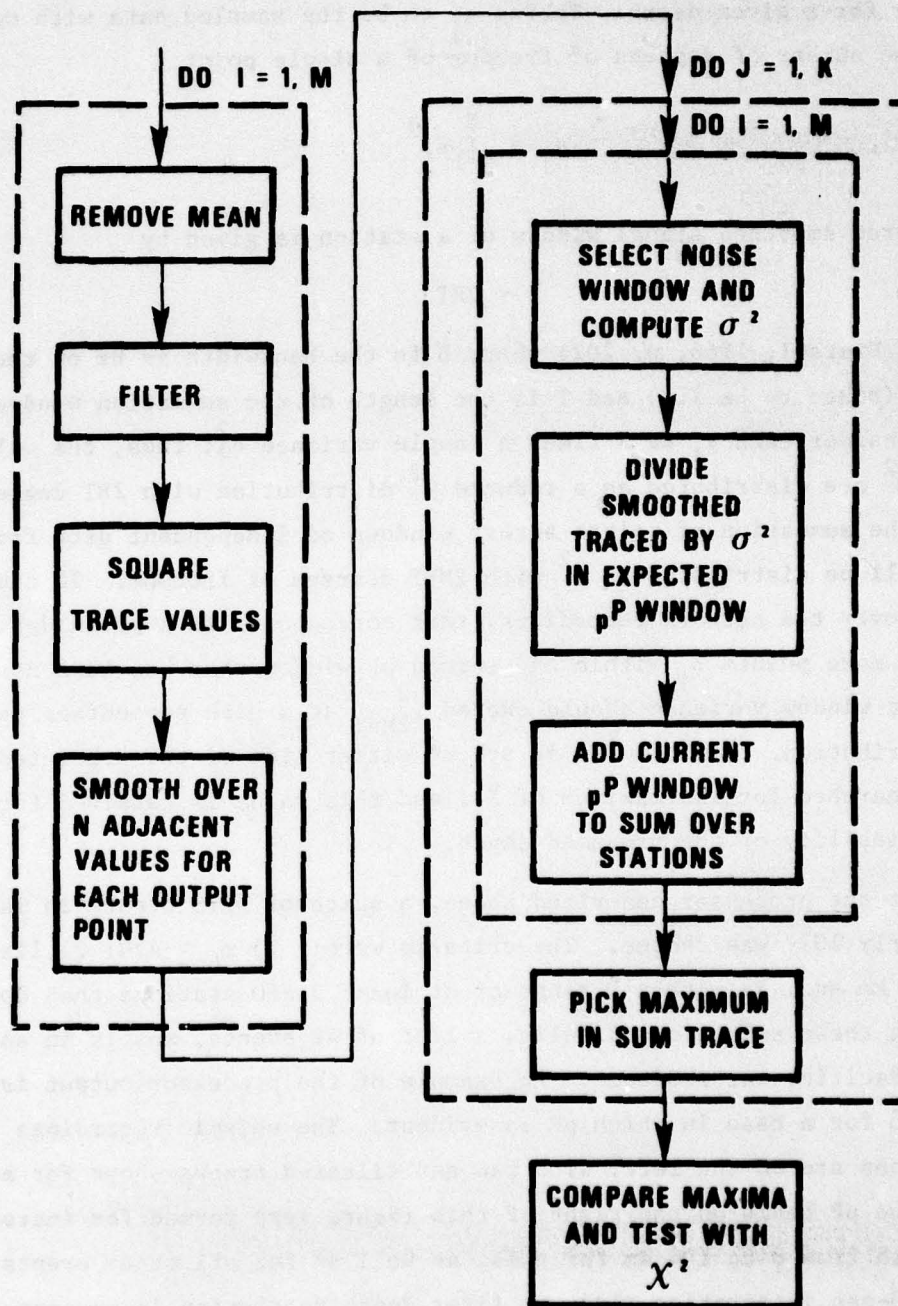


Figure 14. Schematic for the program PPBEAM, an automatic depth determination algorithm.

beyond the presumed pP. During this entire selection procedure no window will be permitted that would include the predicted PcP time for the assumed depth. Stations lacking a satisfactory noise window will be deleted from the beaming for a given depth. Taking s_j to be the sampled data with mean removed, the number of degrees of freedom of a single point

$$y_j = \sum_{j=1}^N s_j^2$$

in the squared smoothed signal window of a station is given by

$$\nu = 2BT$$

(Bendat and Piersol, 1966, p. 202) where B is the bandwidth in Hz of the filtered data (taken to be 1.0) and T is the length of the summation window (here 3 sec). Consider each y_j as N times a sample variance σ_j^2 ; thus, the values $Z_j = N\sigma_j^2/\sigma^2$ are distributed as a reduced χ^2 distribution with 2BT degrees of freedom. The summation of points across windows of independent data for M stations will be distributed as χ^2 with 2MBT degrees of freedom. If there is pP present over the network recordings, that corresponds to a given depth, then one or more points Z_j within the summed pP window that has been normalized by the noise window variance should exceed χ_{2MBT}^2 at a high percentage point of the distribution. A window of ± 2 sec on either side of the predicted pP window is searched for the maximum of Z_j , and this value is retained for the test of reliability of the presumed depth.

To test the processor described above, a suite of NEIS events in late 1976 and early 1977 was chosen. The criteria were: 1) $m_b \geq 4.8$; 2) listed depth < 100 km and, 3) within P range of at least 3 SRO stations then operating. Using these selection criteria, a list of 42 events, mostly in and around the Pacific, was produced. An example of the processor output is shown in Figure 15 for a case in which pP is evident. The seismic recordings from 4 SRO stations are on the left, with raw and filtered traces shown for each station. The pP beams on the right of this figure were formed for increments of 8 km depth from 8 to 104 km for this, as well as for all other events. Due to the 3-sec integration windows, finer depth resolution is unwarranted. The maximum Z_j values in the pP sum window, which are centered on the tick

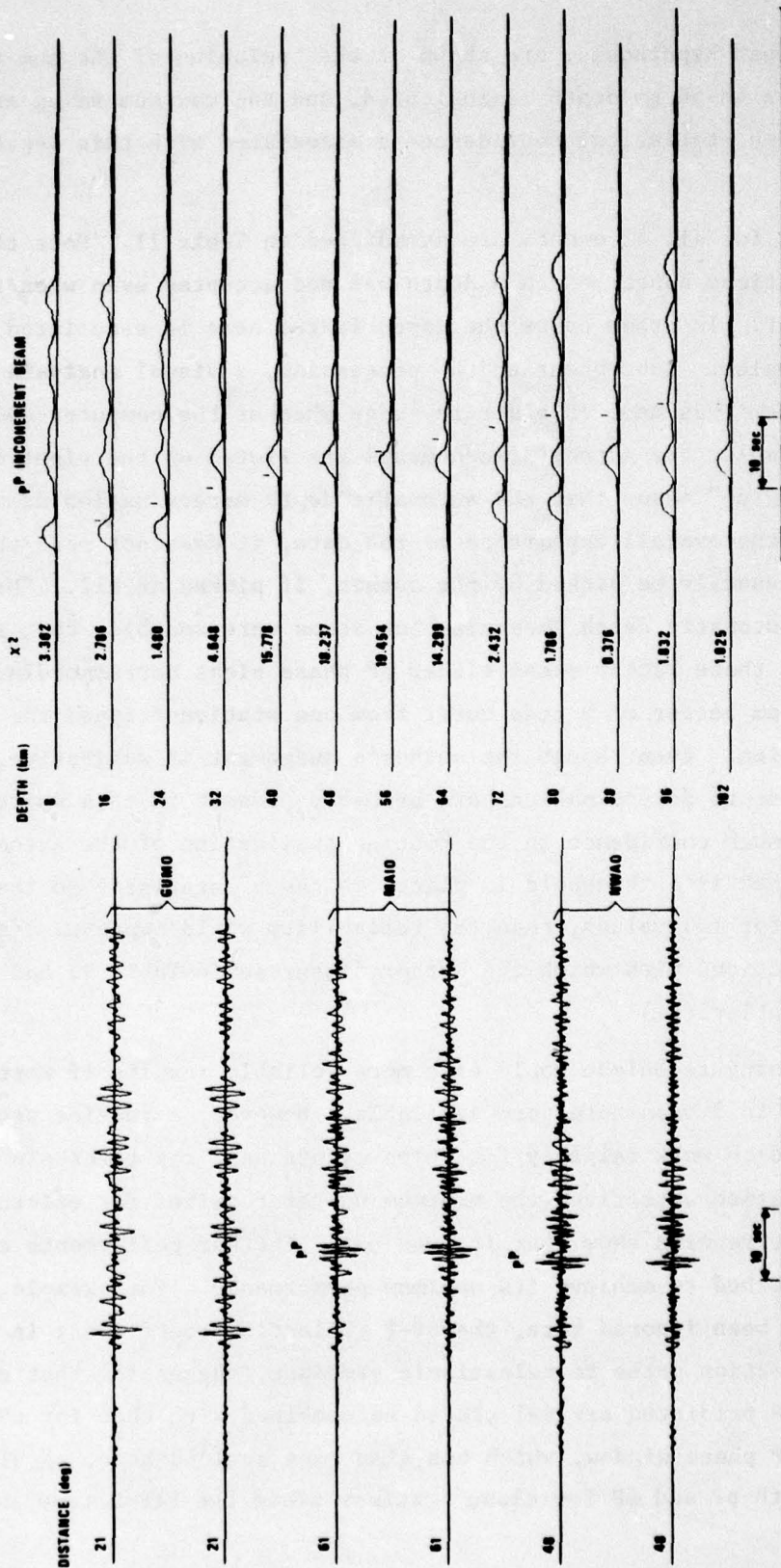


Figure 15. Example of the pP incoherent beamforming for depth determination.

mark for each depth hypothesis, are shown at the beginning of the sum traces. For this event, a 48-56 km depth is indicated, and the maximum value exceeds $\chi^2_{.999}$ so that high statistical confidence is associated with this depth preference.

The results for all 42 events are summarized in Table II. Note that no 8-km depth selections appear; such a depth was not accepted even when its χ^2 value was largest. In other cases the depth listed here is associated with the maximum χ^2 value. Subsequent to the processing, a visual analysis of the plotted seismograms was made in order to judge whether the computer-selected depth was reasonable; the author's judgements are listed on the right of the table. While "agree" means that the automatic depth determination seems reasonable from the overall appearance of the data, it does not mean that this depth would necessarily be picked by the author, if picked at all. "Disagree" means that the automatic depth determination seems unreasonable; that is, a false alarm. In these latter cases either pP phase picks corresponding to another depth seem better or a coda burst from one station tripped the automatic determination. Even though the author's judgement is subjective, too many inaccurate depth determinations are probably present in this suite of events to leave much confidence in the routine application of the automatic process. Note that if a threshold is placed on the χ^2 statistic so that depth is not assigned for low values, then the reliability would improve. (In fact, those depth selections with which the author disagreed in Table II had generally lower χ^2 statistics.)

This processing technique would give more reliable results if more stations than the 3 to 5 used here were available. However, a routine processor would be required to work reliably for those events near the threshold of the network for 3-station detection (the minimum number required for epicenter location) and our results show that it does not. Further refinements are needed for the method to achieve its optimum performance. For example, while the sP phase has been ignored here, the SV-P reflection coefficient is > 0.5 for surface reflection paths to teleseismic stations, suggesting that a window around the sP predicted arrival should be combined with that for pP. In addition, the PcP phase window, which has also been avoided here, should be combined with both pP and sP for close stations since the PcP-P time is

TABLE II

Depth Estimation Results from the
Automatic pP Beamforming Program PPBEAM

<u>Event</u>	<u>#Stations</u>	<u>SRO Depth</u>	<u>Bulletin Depth</u>	<u>χ^2</u>	<u>Analyst</u>	
					<u>Agree</u>	<u>Disagree</u>
210-1	4	32	0	3.2		X
210-2	4	24	0	13.7		X
159-3	3	32	0	4.3		X
159-2	3	40	0	6.0	X	
230-2	4	56	45	8.7		X
229-1	3	16	0	7.6	X	
230-1	3	56	0	7.1	X	
229-3	4	40	0	40.5		X
230-4	3	24	0	5.1	X	
231-1	3	64	0	5.3	X	
232-4	3	56	0	19.5	X	
236-1	4	64	0	4.2	X	
280-1	4	88	117	34.3	X	
258-2	4	16	105	22.7	X	
230-3	3	48	0	7.6	X	
252-1	3	16	67	6.7		X
245-1	5	16	0	5.9		X
242-1	3	48	0	6.6	X	
282-1	3	80	0	10.8	X	
273-5	3	16	0	11.1	X	
279-4	4	24	0	5.5		X
345-1	3	16	0	6.0		X
275-2	3	24	0	5.5	X	
313-2	4	48	0	13.8	X	
337-1	3	48	96	25.8	X	
323-4	4	32	0	10.8	X	
357-1	3	16	0	17.9	X	
326-1	4	16	63	13.3		X

61

TABLE II (cont'd)

<u>Event</u>	<u>#Stations</u>	<u>SRO Depth</u>	<u>Bulletin Depth</u>	<u>χ^2</u>	<u>Analyst</u>	
					<u>Agree</u>	<u>Disagree</u>
312-2	3	16	0	4.0		X
312-1	5	56	73	14.0		X
315-1	3	56	81	9.1	X	
323-2	3	32	75	5.6	X	
348-1	3	16	55	9.8		X
15-2	4	16	0	10.3		X
6-1	4	72	0	5.9	X	
15-1	3	16	0	5.1		X
349-1	5	48	0	6.8	X	
1-2	3	32	0	7.6	X	
17-1	5	16	76	4.6		X
337-1	4	48	96	25.7	X	
342-1	4	32	0	7.6	X	
320-2	4	32	0	10.0	X	

"Agree" - means automatic depth is reasonable from seismogram appearance but not necessarily affirmed to be true

"Disagree" - means automatic depth seems unreasonable from seismogram appearance (false alarm) or that another depth would be picked by analyst (only a few cases)

dependent on depth at regional distance. Therefore, the processor described and tested here could function best as an analyst aid in depth determination, with automatic results checked against the waveforms themselves for each event.

ESTIMATION OF m_b

Justification for a Spectral Estimate

Traditionally, the reported amplitude measurements for seismic phases are based on human measurements of amplitudes on seismic recordings. This body of measurements rests on the application of loose guidelines regarding what exactly is to be measured combined with individual, subjective judgements. This author's experience indicates that amplitude measures made for the purpose of computing m_b may often differ among individuals. Compounding the uncertainty is the even more subjective measurement of the period in order to apply the instrument response correction to obtain true ground displacement. If, in addition, the A/T ratio is formed, error in the period enters a second time to further bias the result used in the standard m_b formula

$$m_b = \log_{10}(A/T) + B \quad (1)$$

where T is the measured period, A is the ground displacement computed at that period from the maximum recorded amplitude, and B is the distance-correction term. A number of automatic procedures (reviewed in Bath, 1975) have been suggested for measuring magnitude. Unfortunately, in this author's opinion, most attempt in some manner or other to simulate the human type of measurement or simply extend it to include more cycles of motion. Attempts to retain the A/T mode of result through automatic procedures are especially undesirable in light of the background rationale for it. In assembling data for the implementation of a magnitude scale for teleseisms, Gutenberg (1945) was confronted with measurements made from many diverse instruments, mostly with broad-band or long-period band responses unlike the typical short-period responses from which m_b is now derived. He found that by dividing amplitude by period T, the values of m_b computed for one event had less scatter than if they were not corrected. This finding is consistent with current source spectral theories in which the spectrum fall-off is f^{-1} , or more, for frequencies

Bath, M., 1975. Spectral Analysis in Geophysics: New York, N. P.

Gutenberg, B., 1945. Amplitudes of P, PP, and S and magnitude of shallow earthquakes, Bull. Seism. Soc. Am., 35, 117-130.

beyond the lowest corner frequency (Geller, 1976). Then, dividing by T , Gutenberg effectively corrected the measurements for the inherent source spectrum although, to be precise, the divisor should be perhaps T^2 or even T^3 . There is little obligation to continue this A/T measure now that almost all m_b 's are derived from narrow-band short-period recordings, such as for the WWSSN or SRO stations, and now that reported periods outside the range 0.5 to 2.0 seconds are rare, usually associated with very large earthquakes or small locally recorded events.

Support for the A/T measure is frequently justified with the argument that the units are conveniently related to energy by squaring. This point is specious, and it was best refuted by Richter (1964), who pointed out "why I have objected strenuously to attempts to assert that the magnitude is definitely a measure of energy...." The magnitude scales were not intended to relate to energy, although it has been used universally in this manner (even by Richter), because it reflects a measure of only a small portion of the total spectrum of an earthquake.

Spectral m_b Definition

With the availability of seismic data in digital form, more precise and objective measurements of magnitude seem possible, with the analyst's role confined to review and approval and occasional resetting of parameters, such as the time window for the measurement. However, any newly suggested magnitude measurement should be rigorously defined and tested, and at least meet these criteria:

- 1) shows high correlation with present m_b estimates in order to maintain a proper accumulation of statistics for recurrence curves and intensity predictions, which can then be easily linked to past data;
- 2) shows equal or less scatter among stations for events than routine m_b ;

Geller, R. J., 1976. Scaling relations for earthquake source parameters and magnitude, Bull. Seism. Soc. Am., 66, 1501-1524.

Richter, C. F., 1964. Historical background of the magnitude scale, in Proceedings of the VESIAC Conference on Seismic Event Magnitude Determination, Acoustics and Seismics Laboratory, University of Michigan, Ann Arbor, Michigan.

- 3) be robust in the presence of spectral nulls, especially for explosions;
- 4) not impair the power of the M_s vs. m_b discriminant between earthquakes and explosions;
- 5) not raise thresholds for reporting m_b .

We propose here a displacement spectral density estimate near 1 Hz as a basis for automated magnitude reporting and we will show how it meets the above criteria. The procedure in computing the proposed measure is to first approximate the continuous transform of the signal

$$A(f) = \frac{1}{T} \int_0^T s(t) e^{-i\omega t} dt$$

by using the Fast Fourier Transform

$$A(n \cdot \Delta f) = \frac{1}{N} \sum_{j=1}^N s(j \cdot \Delta t) e^{-i2\pi n \Delta f j \Delta t}$$

where T is the length in seconds, N is the number of points in T seconds, Δf is the frequency increment, equal to the sampling rate divided by N and Δt is the sampling interval. The discrete representation of the true displacement spectral density results when the instrument I_n is removed by using

$$D(n \cdot \Delta f) = A(n \cdot \Delta f) / I(n \cdot \Delta f)$$

The mean displacement spectral density within a spectral band is given by

$$\bar{D} = \frac{T}{NF} \sum_{n=n_1}^{n_2} D(n \cdot \Delta f) \quad (2)$$

where NF is the number of frequencies summed over. Several experiments with this spectral amplitude measure for m_b are described below and, although the details differ somewhat, the actual frequency bands used all lay within 0.5 to 2.0 Hz and the time window was always 6.4 seconds.

This proposed magnitude measure is simple and its advantages immediately apparent:

- 1) it is an objective method, purposely devoid of options or interactive parameters;
- 2) the resulting D should be independent of instrument response;
- 3) it can be related to long-period spectral level, exactly so if the lowest corner frequency of the event is beyond 2 Hz;

- 4) it avoids m_b -dependent station corrections (Husebye et al., 1974) since the frequency band used is constant with magnitude, unlike the frequency content of time-domain recorded amplitudes;
- 5) it provides data easily compatible with numerous spectral source theories and should permit a clearer judgement on their usefulness;
- 6) it avoids the entire set of problems connected with the routine period measurement for m_b .

Results for Spectral m_b

A pilot analysis of the spectral m_b estimate was made to check its properties, especially its correlation with routine m_b estimates made by a human analyst. A suite of P waves from over 100 earthquakes in 1976 (plotted in Figure 16), as recorded at the SRO station ANMO (Albuquerque, New Mexico), were processed by an interactive graphics program that permitted the analyst to measure amplitude and period in the normal manner and to set the window at the P-wave arrival for the spectral estimate. The analyst-picked amplitude and period quantities were displayed immediately; spectral estimates of the signal and a noise sample in front were also displayed subsequent to the Fourier transformation. For the analyst measures, m_b was computed using equation (1). (In this experiment relative, not absolute, spectral units were computed.) The actual frequency band used was .78 - 1.41 Hz, which comprised 5 spectral points (20 s/sec data). The correlation plot of the analyst m_b versus spectral m_b is shown in Figure 17. A spectral estimate was available for every analyst m_b estimate. The correlation coefficient of .90 is good, but not excellent; the largest deviation from the maximum-likelihood linear fit (based on assumed equal variance for errors in both variables) is 0.8. The 1.04 slope indicates that the spectral measure has little or no magnitude-dependent bias relative to the routine m_b measure, which is an important result in terms of using spectral magnitude for seismic recurrence curves. Two other frequency-band spectral magnitudes were computed --for .31 to .62 Hz and 1.6 to 3.0 Hz. In both cases the correlation with routine m_b estimates

Husebye, E. S., A. Dahle, and K. A. Berteussen, 1974. Bias analysis of NORSAR and ISC Reported seismic event m_b magnitudes, J. Geophys. Res., 79, 2967-2978.

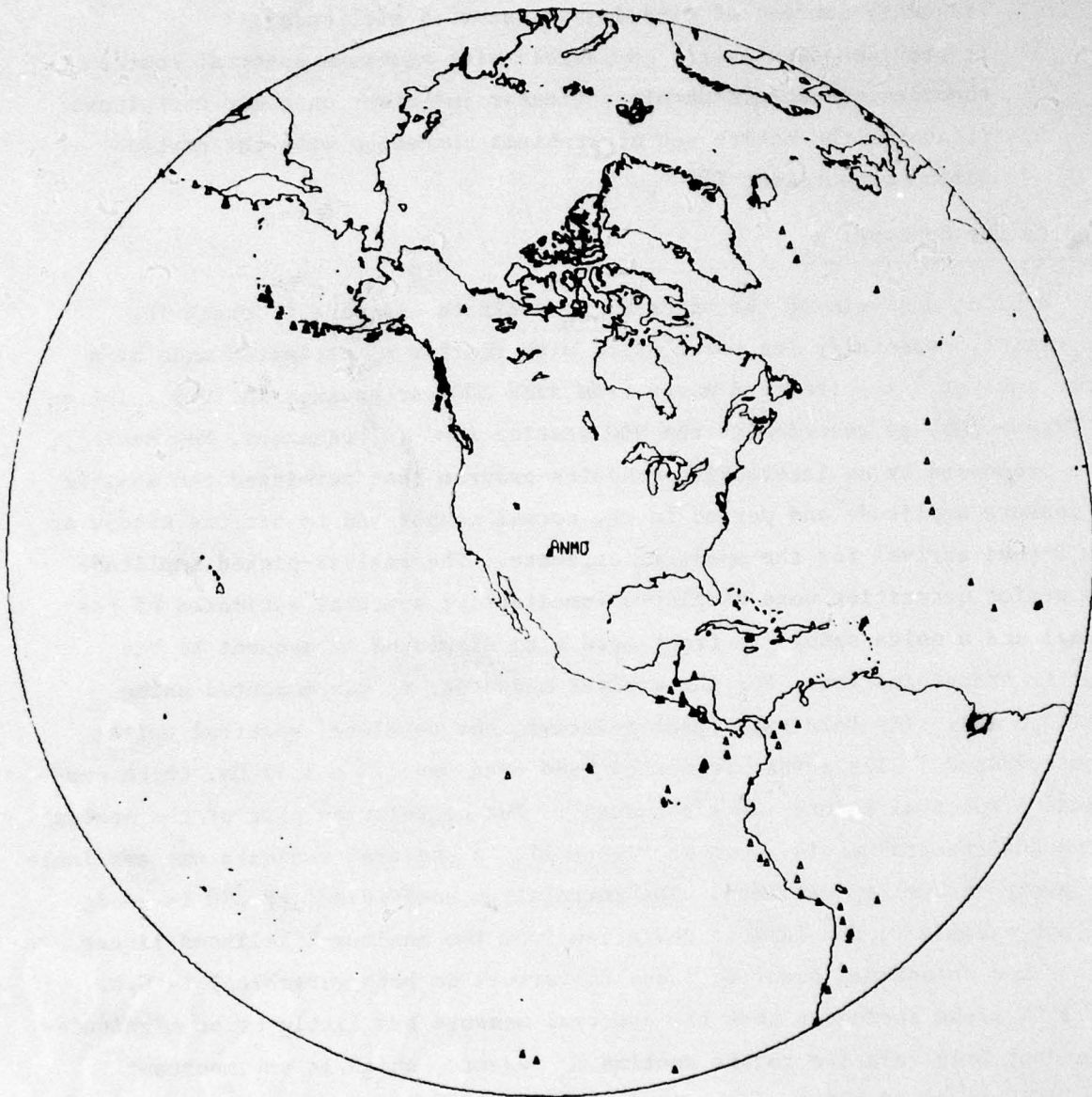


Figure 16. Earthquakes recorded at ANMO and used in determining correlation of spectral-domain and time-domain magnitudes.

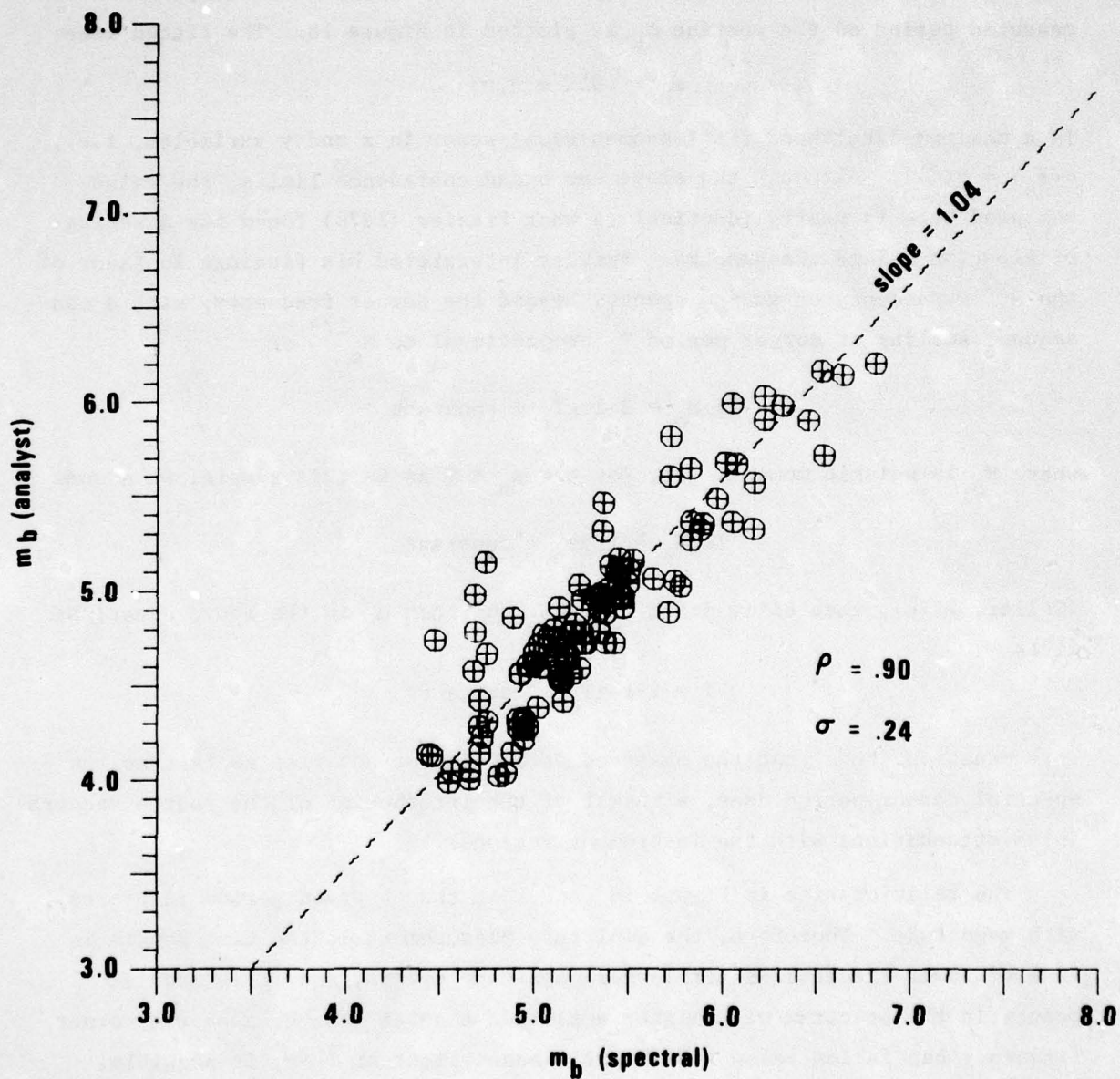


Figure 17. Correlation of spectral-domain and time-domain body-wave magnitude (m_b) at ANMO for events of Figure 16.

was poorer than for the .78 to 1.41 Hz estimates. More significantly, these estimates had many more cases with a $S/N < 2$ than the 0.78 to 1.41 Hz band and, therefore, imply a higher threshold for application.

One interesting outcome related to this experiment is the dependence of measured period on the routine m_b as plotted in Figure 18. The fitted line

$$m_b = .95T + 3.65$$

is a maximum-likelihood fit (assumes equal error in x and y variables, i.e., $\sigma(m_b) = \sigma(T)$). Although the slope has broad confidence limits, the value computed here is nearly identical to what Frazier (1976) found for a series of Aleutian Island aftershocks. Frazier interpreted his findings in favor of the ω^{-3} dependency of source spectra beyond the corner frequency, with a consequent scaling of corner period T_c proportional to $M_o^{1/3}$ or

$$\log M_o = 3 \cdot \log T_c + \text{constant}$$

where M_o is seismic moment. If, for $4 < m_b < 6$ as in this sample, we assume

$$\log M_o \approx 1.5m_b + \text{constant}$$

(Geller, 1976), then elimination of $\log M_o$ and then m_b in the above equations gives

$$T = 2 \cdot \log T_c + \text{constant}$$

This equation shows that the observed period T does not rise as fast as the spectral corner period does, a result of the interaction of the source spectra (plus attenuation) with the instrument response.

The relationships in Figure 18 show that the observed period increases with magnitude. Therefore, the amplitude measurement in the time domain is made at lower frequencies for larger magnitude events, and it is made at points in the spectrum with higher amplitude than at 1 Hz because the corner frequency has fallen below 1 Hz. While measurement at 1 Hz, if possible,

Frazier, C., 1976. Semiannual Technical Summary-Seismic Discrimination, December, 1976, Lincoln Laboratory, MIT, Cambridge, Massachusetts.

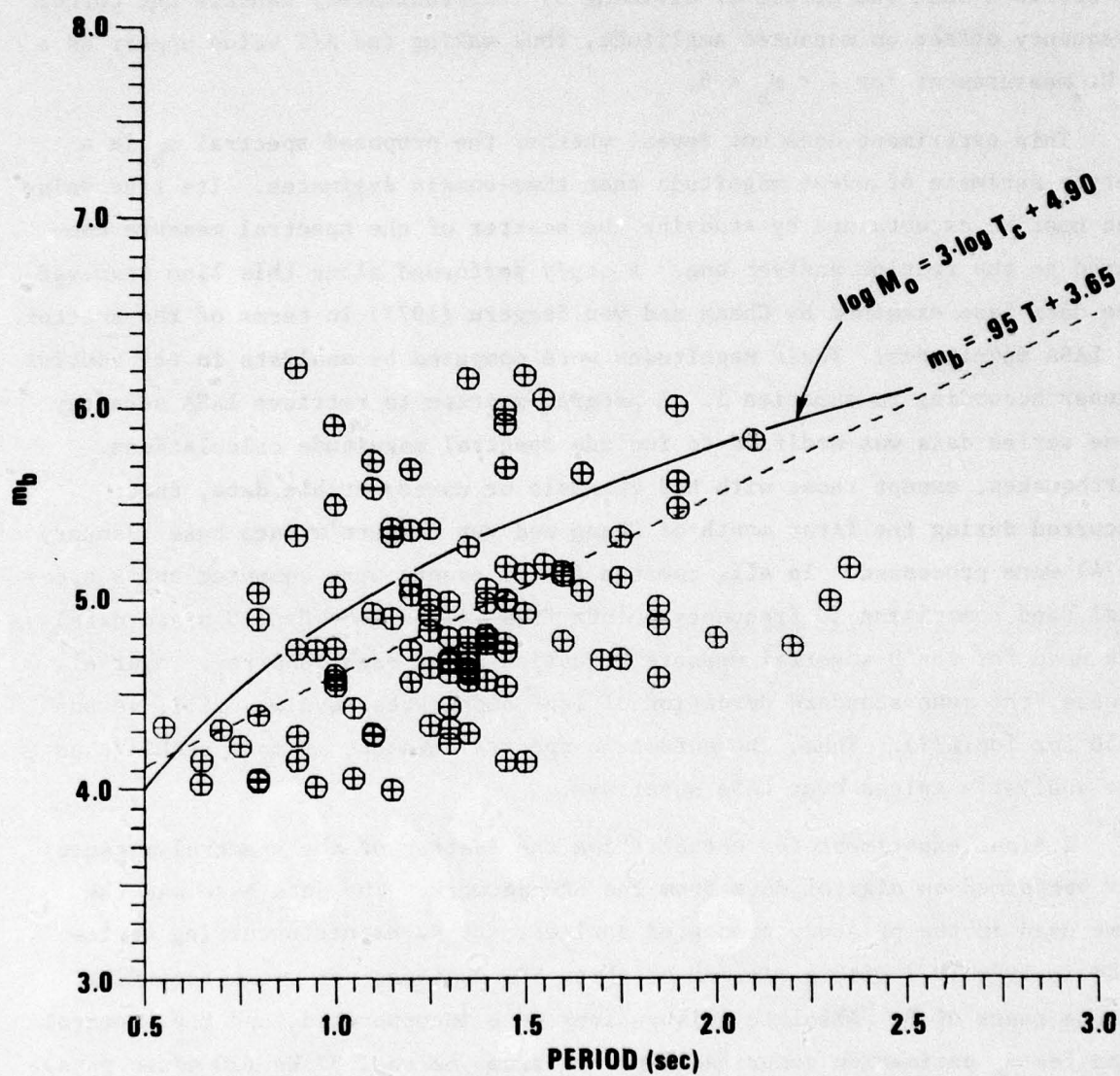


Figure 18. Body-wave magnitude (m_b) versus the observed period at ANMO for events of Figure 16.

would give lower m_b , the higher amplitude is compensated for when dividing by the period to get A/T which is used for magnitude. Since the relationship of spectral m_b (at 1 Hz) and analyst m_b is linear with slope 1 as in Figure 16, we conclude that the effect of dividing by T approximately cancels the corner frequency effect on measured amplitude, thus making the A/T value appear as a 1 Hz measurement for $4 < m_b < 6$.

This experiment does not reveal whether the proposed spectral m_b is a better estimate of event magnitude than time-domain estimates. Its true value can best be ascertained by studying the scatter of the spectral measure compared to the routine analyst one. A study performed along this line involved the data base examined by Chang and von Seggern (1977) in terms of the scatter of LASA magnitudes. Their magnitudes were computed by analysts in the routine manner according to equation 1. A program written to retrieve LASA subarray time series data was modified to include spectral magnitude calculations. Earthquakes, except those with bad channels or unrecoverable data, that occurred during the first month of Chang and von Seggern's data base (January 1974) were processed. In all, spectra for 21 events were computed and a spectral band comprising 10 frequency points from .47 to 1.88 Hz (10 s/sec data) was used for the \bar{D} spectral measure (equation 2) at each subarray. Over all events, the mean standard deviation of $\log \bar{D}$ among subarrays was .112, versus .156 for $\log(A/T)$. Thus, the automatic spectral measure is more stable than the analyst's values over LASA subarrays.

A final experiment for establishing the scatter of the spectral measure was performed on digital data from the SRO network. The data base was the same used in the pP study presented earlier, the 42 events occurring worldwide in 1976-1977 with a minimum of three SRO stations per event recording in the range of P. Absolute calibrations were incorporated, and the spectral band for m_b estimation comprised 8 points from .62 to 1.87 Hz (20 s/sec data). The analyst and spectral m_b 's were computed as in the LASA experiment, with the result that each had an average standard deviation of 0.38 over all 42 events.

Table III summarizes the spectral m_b results compared with routine analyst estimates. The standard deviations of the spectral estimate are as

TABLE III

Automatic Spectral VS. Human Analyst m_b

	<u>LASA Experiment</u>	<u>SRO Experiment</u>
Number Earthquakes	21	42
Number Stations	13	3-6
Passband	0.47 - 1.87 hz	0.62 - 1.87 hz
Analyst Mean $\sigma(\hat{m}_b)$.16	.38
Spectral Mean $\sigma(\hat{m}_b)$.11	.38
Mean $[\hat{m}_b(A) - \hat{m}_b(S)]$	-.24	-.26

low or lower than those of analyst estimates. In the case of the SRO experiment, all the factors contributing to magnitude scatter are present. However, for the LASA experiment, the source radiation pattern and path effects are uniform over all 13 subarrays, with a consequent lessening of the magnitude scatter compared to worldwide sampling. The bias of the spectral m_b , with a mean of roughly -0.25 in both experiments, is expected. This negative bias was fairly consistent over all events, ranging from -0.02 to -0.42 over the 42 earthquakes for which SRO recordings were used. The spectral density near 1.0 Hz is for a narrow-band process with somewhat random phase (typical P wave) and closely represents the rms of the signal whereas the peak amplitude is used in the routine m_b estimation.

ESTIMATION OF M_s

Definition of a Spectral M_s

Using the long-period processing scheme outlined in a previous section, automating the routine estimates of M_s from Rayleigh waves should be possible. The time window that produces the maximum acceptable F-statistic would be used in the estimation. As with m_b , the time-domain measurements are circumvented altogether and we proceed to a spectral amplitude, using a formulation for \bar{D} similar to that already presented for P waves. Criticisms that can be brought against measurements of amplitude and period in the time domain apply equally to surface waves and body waves, and an improved M_s estimate is sought rather than an automated simulation of the sometimes faulty and subjective procedure commonly in use.

In addition to the flaws of time-domain measurements, a further complication exists with surface waves that makes a spectral measure appealing on theoretical grounds. Von Seggern (1971) illustrated the differences in amplitude at $T \approx 20$ sec to be expected for propagation of Rayleigh waves over varying models of the earth's structure, e.g., oceanic, shield, or tectonic. The amplitude difference between deep ocean paths and shield paths is pronounced and it may amount to more than a factor of two. However, the spectral amplitude is more independent of structural type, assuming that attenuation is constant among structures. The stationary-phase approximation (Bath, 1969) relates the time-domain displacement $f(t)$ at frequency ω_0 to the spectral displacement $\hat{f}(\omega_0)$ by

$$|f(t)|_{\omega_0} = 2 \left[\frac{1}{\pi T T \left| \frac{\partial^2 \omega}{\partial k^2} \right|_{\omega_0}} \right]^{1/2} \cdot U(\omega_0) \cdot \hat{f}(\omega_0) \quad (3)$$

von Seggern, D. H., 1971. Effects of propagation paths on surface-wave magnitude estimates, SDL-279, Teledyne Geotech, Alexandria, Virginia.

Bath, M., 1969. Mathematical Aspects of Seismology: New York, Elsevier.

where TT is the travel time and U is group velocity. By definition

$$\frac{\partial \omega}{\partial k} = U$$

$$\frac{\partial^2 \omega}{\partial k^2} = U \frac{\partial U}{\partial \omega}$$

From $\omega = 2\pi/T$, we get

$$\partial \omega = - \frac{2\pi dT}{T^2}$$

By substitution then

$$\frac{\partial^2 \omega}{\partial k^2} = \frac{UT^2}{2\pi} \frac{\partial U}{\partial T}$$

Using this result in equation 3 and changing TT to r/U , we have

$$|f(t)|_{T_0} = 2 \left[\frac{1}{r |dU/dT|_{T_0}} \right]^{\frac{1}{2}} \cdot \frac{U(T_0)}{T_0} \cdot \hat{f}(T_0) \quad (4)$$

At a given period T_0 then, time-domain amplitude depends on the values of U and dU/dT at that period. We shall examine the extremes from von Seggern's (1971) 20 sec period values, which are

$$\text{shield: } dU/dT = .03 \frac{\text{km}}{\text{sec}^2}, \quad U = 3.1 \frac{\text{km}}{\text{sec}}$$

$$\text{ocean: } dU/dT = .25 \frac{\text{km}}{\text{sec}^2}, \quad U = 3.6 \frac{\text{km}}{\text{sec}}$$

Substituting in equation 4, we obtain the possible range in $|f(t)|_{T_0}$:

$$|f(t)|_{T_0=20} \approx \left(\frac{0.72}{1.80} \right) \frac{\hat{f}(T_0)}{r^{\frac{1}{2}}} \quad (5)$$

where r is entered in km and \hat{f} in nm·sec to obtain nm on the left-hand side. The 0.72 factor is for oceans, and 1.80 for shields; nearly all other values derived for any other reasonable earth model would lie within this range. Note that this formula is valid only when the stationary-phase approximation is valid, which is generally true for $T = 20$ sec globally.

The conventional "Prague" formula for M_s (Vanek et al., 1962) is

$$M_s = \log \left[|f(t)|_{T_0} / T_0 \right] + 1.66 \log \Delta + 0.30$$

where $f(t)$ is measured in nm zero-to-peak at the maxima of the Rayleigh wave, provided $17 \leq T_0 \leq 23$ sec, and Δ is in degrees of epicentral distance. By using equation 5, and putting $T_0 = 20$ sec, we can convert to spectral displacement density thus

$$M_s' = \log \left[\left(\frac{0.72}{1.80} \right) \frac{\hat{f}(T_0)}{r^{1/2}} \right] + 1.66 \log \Delta - 1.00$$

The distance r in km can be converted to degrees and absorbed into the last two terms to obtain

$$M_s' = \log \left[\left(\frac{0.72}{1.80} \right) \hat{f}(T_0) \right] + 1.16 \log \Delta - 2.02$$

Let us assume a mean value of 1.2 for the structure-dependent factor which ranges from 0.72 to 1.80, and the final spectral formula for M_s is

$$M_s' = \log \left[\hat{f}(T_0) \right] + 1.16 \log \Delta - 2.24 \quad (6)$$

For a seismic event, this equation should result in a network mean magnitude compatible with the classically determined one. Note that $Q \sim 350$ is implicit in the distance-correction term in this equation (von Seggern, 1971). Thus, by using spectral magnitudes based on $\bar{D} = \hat{f}(T_0)$ averaged over a band near 20-sec period, some scatter may be eliminated that results from dispersion effects on time-domain amplitudes. In addition, the values of \bar{D} have for M_s all the desirable properties ascribed to the P-wave spectral estimate for m_b , except for perhaps item 4.

Results for Spectral M_s

Before applying the spectral measure to the estimation of M_s , a pilot project to determine the correlation between the proposed LR spectral magnitude and the analyst's routine estimates of M_s was performed. This experiment was based on the same epicenters (Figure 16) used in the m_b pilot project and again the SRO recordings at ANMO. The interactive graphics package allowed the

Vanek, J., A. Zatopek, V. Karnik, N. V. Kondorskaya, Yu. V. Riznichenko, E. F. Savarensky, S. L. Solov'yev, and N. V. Shebalin, 1962. Standardization of magnitude scales, Bull. Acad. Sci. USSR, Geophys. Series, 108-111.

analyst to measure amplitude and period in the normal manner as described for the m_b study and to set the window (512 sec) for the spectral computations on the LR wave. Spectral amplitude was averaged in three passbands, but only the center band from .0390 to .0469 Hz (5 spectral points for 1 sample/sec data) was used to present results here since S/N ratios were highest in it. Conventional M_s was computed according to the "Prague" formula given above and spectral M_s was computed according to equation 6 with an arbitrary constant added to produce the plot in Figure 19 of spectral versus analyst M_s for 106 earthquakes. The high correlation and apparently linear trend over the entire magnitude range represented here indicates that the spectral measure could be adopted without seriously biasing individual event magnitudes or earthquake statistics based on M_s .

A second experiment involved the comparison of spectral M_s scatter and analyst M_s scatter over the NORSAR long-period array. Ten large events were selected at $\Delta > 40^\circ$, and the quantities $\log(\bar{D})$ and $\log(A/T)$ were computed for each of the 22 sensors for these events. No distance correction was necessary to get relative M_s over the NORSAR array because the amplitude loss with distance is negligible within 100 km. The standard deviations of $\log(A/T)$ and $\log(\bar{D})$ were averaged with the result shown in Table IV. Since the spectral measure has a slightly lower variance, it provides an equal or more consistent estimate of the surface-wave magnitude.

In order to compare M_s and M_s' directly, the SRO data for six large explosions in 1976 was processed. \bar{D} was estimated by the average displacement spectral density in the .03 to .05 Hz band, which is a band shifted to lower frequencies than at $T = 20$ sec. The results are given in Table IV. Using the spectral estimate, no significant decrease in the typical magnitude scatter was found; these results were similar to findings over the NORSAR array. However, in using worldwide sites, rather than an array, the magnitude scatter is expected to be large because of differential source, path, and receiver effects, whose cumulative effect apparently overwhelms any possible improvement in station magnitude estimation made with a spectral measurement of the signal amplitude. A much larger sample of events is needed to conclusively demonstrate the anticipated small reduction in scatter with spectral M_s . Note the negative bias of the spectral M_s in Table IV; this may be due to a multiplicative

error in the relation between spectral-domain and time-domain amplitude given in equation 5.

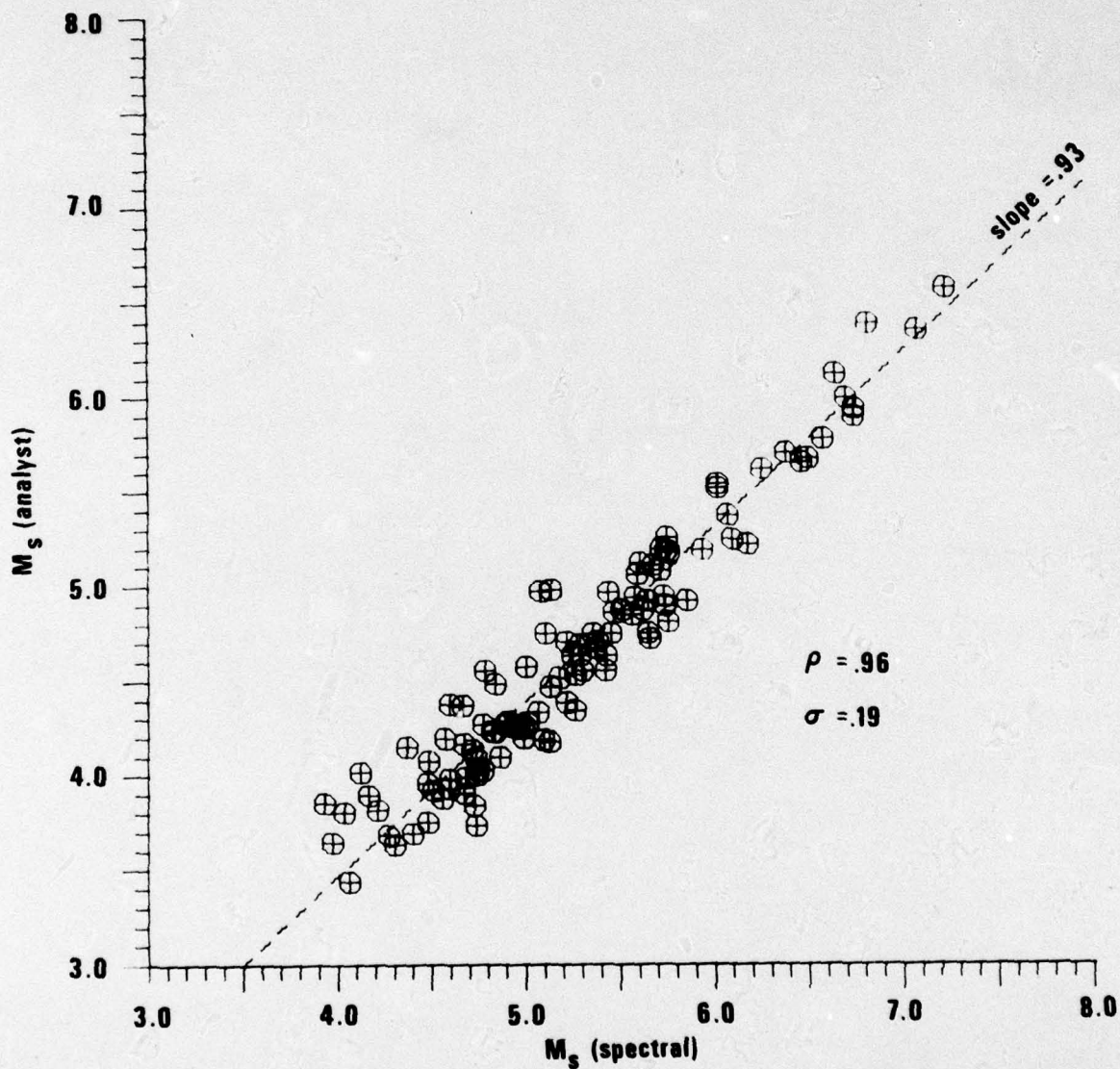


Figure 19. Correlations of spectral-domain and time-domain surface-wave magnitude (M_s) at ANMO for events of Figure 16.

TABLE IV

Automatic Spectral VS. Human Analyst M_s

	<u>NORSAR Experiment</u>	<u>SRO Experiment</u>
Number Earthquakes/Explosions	10 EQ	6 EX
Number Stations	22	5-12
Passband	.031 - .050 hz	.031 - .050 hz
Analyst Mean $\sigma(\hat{M}_s)$.089	.22
Spectral Mean $\sigma(\hat{M}_s)$.075	.19
Mean $[\hat{M}_s(A) - \hat{M}_s(S)]$	—	-.48

CONCLUSION

The capability exists to automate a number of routine seismic analysis tasks performed in the preparation of a global seismic bulletin such as the NEP system produces at the SDAC. The proposed means discussed in this report have been tested and shown to work in an acceptable, but not always fully satisfactory, way. They should function in a context of close analyst scrutiny of the results in order to prevent unrealistic output formed only by machine computations.

Even if the results of automated processing are acceptable, the machine time required is also a factor to be weighed. Calculations in this report were performed on the IBM 360/44 computer with a TS44 operating system. Approximate computation times for the various processes discussed in this report are:

- 1) Fisher verifier - < 10 sec per LASA detection
- 2) PE arrival time - < 5 sec per detection and first motion
- 3) F-statistic for surface waves - < 15 sec per detection
- 4) automatic association - < 1 hr per 24 hrs of detections from numerous sites
- 5) pP enhancement - < 60 sec per event
- 6) spectral m_b or M_s - < 5 sec per signal computation

These estimates are crude because many computations and overhead, which would be superfluous in routine applications, were imbedded in the test programs and because of the inability to estimate accurately that additional time. In all cases, the work can be performed by machine at a comparable or more rapid pace than that of a human analyst.

Results of this study lead to the following recommendations concerning the automation of the NEP bulletin:

- 1) A Fisher-type detection process should be performed on array detections to eliminate several types of false alarms which needlessly augment the detection logs. This process should be cascaded with a spectral ratio check to eliminate high-frequency local and regional events from array detection logs.

- 2) The prediction-error (PE) technique should be implemented and tested in NEP as a means of defining exact start times and the first-motion directions and setting the window gate for a spectral m_b estimate.
- 3) Smart's (1977) surface-wave detector should be implemented and tested on NEP as a means of selecting the window of maximum 20-sec LR amplitude for a spectral M_s estimate. The detector would be initiated at an arrival time crudely defined by the prediction of the global group-velocity grid.
- 4) Automatic association according to the method of keying on array detections, finding other arrivals, and executing HYPO is already installed in NEP. Other automatic methods such as maximum-likelihood hypothesis testing and clustering should be considered if array-type detection information (velocity and azimuth) becomes available to NEP from more sites than at present.
- 5) Some method of graphically aiding the analyst in depth determination should be implemented. The pP beamforming tested here does not seem reliable, and a simpler approach such as waveform displays with expected pP arrival times for any depth selected by the analyst is recommended at present. More on-line experience with pP, sP, and PcP phases should lead to the improvement of the pP beamforming technique presented here.
- 6) Spectral estimates of m_b and M_s , using the displacement density spectrum near 1 Hz and .05 Hz respectively, should be computed for all on-line NEP data in order to build a large data base for extensive comparison with routine methods of magnitude determination.

ACKNOWLEDGEMENTS

This report represents the work and ideas of several people in addition to the author. R. H. Shumway supplied the "dendogram" clustering results for automatic association, and B. R. Carroll is responsible for the programming and implementation of the current automatic association package in NEP. E. Smart kindly allowed his program for LR/LQ detection to be tested here. T. McElfresh wrote the program for automatic depth determination from pP delays. B. Barker was responsible for processing much of the data pertaining to spectral magnitudes. Critical comments by Z. A. Der and R. R. Blandford on this report are much appreciated. This research was supported by the Defence Advanced Research Projects Agency under contract F08606-78-C-0007 under the technical direction of the VELA Seismological Center.

REFERENCES

- Barnard, T. E., and L. J. O'Brien, 1974. An evaluation of adaptive-beamforming techniques applied to seismic data, ALEX(01)-TR-74-08, Texas Instruments, Inc., Dallas, Texas.
- Bath, M., 1975. Spectral Analysis in Geophysics: Elsevier, New York.
- Bath, M., 1969. Mathematical Aspects of Seismology: Elsevier, New York.
- Bendat, J. S., and A. G. Piersol, 1966. Measurement and Analysis of Random Data: John Wiley & Sons, New York.
- Blandford, R. R., 1970. An automatic event detector at TFO, SDL-263, Teledyne Geotech, Alexandria, Virginia. AD 881 923.
- Blandford, R. R., 1972. Qualitative properties of the F-detector, SDL-291, Teledyne Geotech, Alexandria, Virginia. AD 753 059.
- Blandford, R. R., and M. H. Wirth, 1973. Automatic array and network detection in the presence of signal variability, SDL-308, Teledyne Geotech, Alexandria, Virginia. AD 768 927.
- Blandford, R. R., 1975. Use of source-region-station time corrections at NTS for depth estimation, SDAC-TR-75-4, Teledyne Geotech, Alexandria, Virginia. AD 025349.
- Blandford, R. R., and D. Clark, 1975. Variability of seismic waveforms recorded at LASA from small subregions of Kamchatka, SDAC-TR-75-12, Teledyne Geotech, Alexandria, Virginia. AD 028968.
- Bolt, B. A., 1960. Machine processing of seismic travel-time data, Bull. Seism. Soc. Am., 52, 259-268.
- Capon, J., R. J. Greenfield, and R. T. Lacoss, 1969. Long period signal processing results for the Large Aperture Seismic Array, Geophysics, 34, 305-329.
- Chang, A. C., R. M. Seggelke, and R. R. Baumstark, 1976. Analysis and reduction of false alarms at LASA, SDAC-TR-76-6, Teledyne Geotech, Alexandria, Virginia. AD 030766.
- Chang, A. C., and D. H. von Seggern, 1977. A study of amplitude anomaly and m_b bias at LASA subarrays, SDAC-TR-77-11, Teledyne Geotech, Alexandria, Virginia.
- Choy, G., and K. McCamy, 1973. Enhancement of long-period signals by time varying adaptive filters, J. Geophys. Res., 78, 3505-3511.
- Claerbout, J. F., 1964. Detection of P-waves from weak sources at great distances, Geophysics, 29, 197-211.

REFERENCES (Continued)

- Dean, W. C., and R. O. Ahner, 1971. Evaluation of the SAAC/LASA system, SAAC-1, Teledyne Geotech, Alexandria, Virginia.
- De Braemacker, J. C., 1964. Detection of small arrivals, Bull. Seism. Soc. Am., 54, 2141-2164.
- Evernden, J., 1969. Identification of earthquakes and explosions by use of teleseismic data, J. Geophys. Res., 74, 3828-3856.
- Flinn, E. A., 1960. Local earthquake location with an electronic computer, Bull. Seism. Soc. Am., 50, 467-470.
- Frazier, C., 1976. Semiannual Technical Summary-Seismic Discrimination, December 1976, Lincoln Laboratory, MIT, Cambridge, Massachusetts.
- Geller, R. J., 1976. Scaling relations for earthquake source parameters and magnitude, Bull. Seism. Soc. Am., 66, 1501-1524.
- Geotech, 1968. ADAPS, an automatic data association and processing system for seismological data. Volume 3, Program descriptions, TR-68-28, Teledyne Geotech, Garland, Texas.
- Gjoystaal, H., and E. S. Husebye, 1972. A comparison of performance between prediction error and bandpass filters, NORSAR Technical Report No. 48, NTN/NORSAR, Kjeller, Norway.
- Gutenberg, B., 1945. Amplitudes of P, PP, and S and magnitude of shallow earthquakes, Bull. Seism. Soc. Am., 35, 117-130.
- Gutenberg, B., and C. F. Richter, 1954. Seismicity of the Earth, 2nd edition: Princeton University Press. Princeton, New Jersey.
- Husebye, E. S., A. Dahle, and K. A. Bertheussen, 1974. Bias analysis of NORSAR and ISC reported seismic event m_b magnitudes, J. Geophys. Res., 79, 2967-2978.
- Kovacs, P., 1966. LOCAS, a system for processing seismic arrival data (U), Report No. TR-66-103, Teledyne Geotech, Garland, Texas, (Classified).
- Lambert, D. G., D. H. von Seggern, S. S. Alexander, and G. A. Galat, 1969. The Long Shot experiment, Volume II, Comprehensive analysis, SDL-234, Teledyne Geotech, Alexandria, Virginia. ADA 698 319.
- Lomnitz, C., 1977. A procedure for eliminating the indeterminacy in focal depth determinations, Bull. Seism. Soc. Am., 67, 533-535.
- Massé, R. P., 1975. A technique for computing surface-wave properties, Bull. Seism. Soc. Am., 65, 1743-1751.

REFERENCES (Continued)

- Moltshan, G. M., V. F. Pisarenko, and N. A. Smirnova, 1964. Some statistical methods of detecting signals in noise, Geophys. J., 8, 319-323.
- Muirhead, K. J., and R. Datt, 1976. The N-th root process applied to seismic array data, Geophys. J., 47, 197-210.
- Richter, C. F., 1964. Historical background of the magnitude scale, in Proceedings of the VESIAC Conference on Seismic Event Magnitude Determination, Acoustics and Seismics Laboratory, University of Michigan, Ann Arbor, Michigan.
- Shlien, S., and M. N. Toksöz, 1973. Automatic event detection and location capabilities of large aperture seismic arrays, Bull. Seism. Soc. Am., 63, 1275-1288.
- Shlien, S., and M. N. Toksöz, 1974. Automatic phase identification with one and two large aperture seismic arrays, Bull. Seism. Soc. Am., 64, 221-234.
- Shoup, E. M., and R. L. Sax, 1975. Simulation of a world-wide seismic surveillance network, ALEX(01)-TR-74-13, Texas Instruments, Inc., Dallas, Texas.
- Simons, R., 1968. PHILTRE-A surface wave particle motion discrimination process, Bull. Seism. Soc. Am., 58, 629-637.
- Smart, E., 1977. A 3-component, single-station, maximum-likelihood surface-wave detector, SDAC-TR-77-14, Teledyne Geotech, Alexandria, Virginia.
- Stewart, S. W., 1977. Real-time detection and location of local seismic events in central California, Bull. Seism. Soc. Am., 67, 433-452.
- Ulrych, T. J., and T. N. Bishop, 1975. Maximum entropy spectral analysis and autoregressive decomposition, Rev. Geophys., 13, 183-200.
- Vanek, J., A. Zatopek, V. Karnik, N. V. Kondorskaya, Yu. V. Ryznichenko, E. F. Savarensky, S. L. Solovyev, and N. V. Shebalin, 1962. Standardization of magnitude scales, Bull. Acad. Sci. USSR, Geophys. Series, 108-111.
- von Seggern, D. H., 1971. Effects of propagation paths on surface-wave magnitude estimates, SDL-279, Teledyne Geotech, Alexandria, Virginia. AD 739 180.

REFERENCES (Continued)

- von Seggern, D. H., 1976. Final report on the analysis of recordings from the Very Long Period Experimental stations, SDAC-TR-76-1, Teledyne Geotech, Alexandria, Virginia. (Classified)
- Weichert, D. H., and M. Henger, 1976. The Canadian Seismic array monitor processing system (CANSAM), Bull. Seism. Soc. Am., 66, 1381-1404.
- Williams, W. T., and G. N. Lance, 1977. Hierarchical classificatory methods, in Statistical Methods for Digital Computers, ed. K. Enslien et al.: John Wiley & Sons, New York.